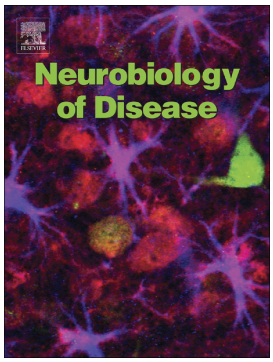

Characterization of tau binding by gosuranemab

Richelle Sopko, Olga Golonzhka, Joseph Arndt, Chao Quan, Julie Czerkowicz, Andrew Cameron, Benjamin Smith, Yogapriya Murugesan, Garrett Gibbons, Soo-Jung Kim, John Q. Trojanowski, Virginia M.Y. Lee, Kurt R. Brunden, Paul H. Weinreb, Danielle L. Graham, Heike Hering

PII: S0969-9961(20)30395-8

DOI: https://doi.org/10.1016/j.nbd.2020.105120

Reference: YNBDI 105120

To appear in: *Neurobiology of Disease*

Received date: 28 May 2020

Revised date: 11 September 2020

Accepted date: 24 September 2020

Please cite this article as: R. Sopko, O. Golonzhka, J. Arndt, et al., Characterization of tau binding by gosuranemab, *Neurobiology of Disease* (2020), https://doi.org/10.1016/j.nbd.2020.105120

Characterization of tau binding by gosuranemab

Richelle Sopko[a,*], Olga Golonzhka[a], Joseph Arndt[a], Chao Quan[a], Julie Czerkowicz[a], Andrew Cameron[a], Benjamin Smith[a], Yogapriya Murugesan[a], Garrett Gibbons[b], Soo-Jung Kim[b], John Q. Trojanowski[b], Virginia M.Y. Lee[b], Kurt R. Brunden[b], Paul H. Weinreb[a], Danielle L. Graham[a], Heike Hering[a]

[a] *Biogen, Cambridge, MA, USA*

[b] *Center for Neurodegenerative Disease Research, University of Pennsylvania, Philadelphia, PA, USA*

*Corresponding author at: Biogen, 225 Binney Street, Cambridge, MA 02142, USA.

E-mail address: richelle.sopko@biogen.com

Word count: 9956 words

Figures/tables: 8 Figures, 5 Tables, 7 Supplementary Figures, 6 Supplementary Tables

Abbreviations

AD, Alzheimer's disease; BSA, bovine serum albumin; CBD, corticobasal degeneration; CDR, complementarity-determining region; CSF, cerebrospinal fluid; ELISA, enzyme-linked immunosorbent assay; FACS, fluorescence-activated cell sorting; F_{norm}, fluorescence intensity after thermophoresis/fluorescence intensity before thermophoresis; FRET, fluorescence resonance energy transfer; HRP, horseradish peroxidase; HTS, High Throughput Sampler; HV, healthy volunteer; ISF, interstitial fluid; K_D, dissociation constant; MST, microscale thermophoresis; nY18, nitrated Y18; PBS, phosphate-buffered saline; PBS-T, PBS, 0.05% Tween-20; PFF, preformed fibrils; PSP, progressive supranuclear palsy; pY18, phosphorylated Y18; RD, repeat domains.

Abstract

Deposition of tau aggregates in the brain is a pathological hallmark of several neurodegenerative diseases, termed tauopathies, such as Alzheimer's disease (AD), corticobasal degeneration, and progressive supranuclear palsy (PSP). As transcellular spread of pathological tau aggregates has been implicated in disease progression, immunotherapy is being considered as a treatment for tauopathies. Here we report a detailed biochemical and biophysical characterization of the tau-binding properties of gosuranemab, a humanized monoclonal antibody directed against N-terminal tau that is currently being investigated as a treatment for AD. Binding experiments showed that gosuranemab exhibited high affinity for tau monomer, tau fibrils, and insoluble tau from different tauopathies. Epitope mapping studies conducted using X-ray crystallography and mutagenesis showed that gosuranemab bound to human tau residues 15–22. Immunodepletion of pathological human brain homogenates and transgenic mouse interstitial fluid (ISF) with gosuranemab resulted in reduced tau aggregation in tau biosensor cells. Preincubation of seed-competent AD-tau with gosuranemab significantly inhibited tau aggregation in mouse primary cortical neurons. Gosuranemab also significantly reduced unbound N-terminal tau in cerebrospinal fluid (CSF) from individuals with PSP and AD, and in ISF and CSF of treated transgenic mice. These results are consistent with the >90% target engagement observed in the CSF of some clinical trial dosing cohorts and support the evaluation of gosuranemab as a potential treatment for AD.

Keywords: Affinity; antibody; gosuranemab; immunotherapy; tau; tauopathies

1. Introduction

Tau is an abundant neuronal protein with multiple cellular functions. Originally described as a microtubule-associated protein predominantly found in axons, tau plays a role in regulating microtubule dynamics (Guo et al., 2017); however, low levels of tau are found in dendrites and might also be involved in postsynaptic signaling (Arendt et al., 2016). More recently, cytosolic tau has also been implicated in the regulation of RNA binding proteins, and nuclear tau in the regulation of heterochromatin stability and nuclear import (Eftekharzadeh et al., 2018; Mansuroglu et al., 2016; Vanderweyde et al., 2016). In its native state, tau is soluble, highly disordered, and lacks a well-defined three-dimensional structure (Zabik et al., 2017). It is primarily an intracellular protein, but neurons also release tau into the extracellular space under physiological conditions and tau release is enhanced by increased neuronal activity (Karch et al., 2012; Pooler et al., 2013; Wu et al., 2016; Yamada et al., 2014). Tau is found in the interstitial fluid (ISF) and cerebrospinal fluid (CSF) of mammals including humans (Bright et al., 2015; Magnoni et al., 2012; Sato et al., 2018; Yamada et al., 2011). Extracellular tau exists predominantly as fragments, with mid-region fragments being at least twice as abundant as N-terminal fragments irrespective of non-disease or disease classification, although full-length species have also been detected (Barthélemy et al., 2016; Bright et al., 2015; Chen et al., 2019; Cicognola et al., 2019; Guix et al., 2018; Karch et al., 2012; Meredith et al., 2013; Sato et al., 2018; Wagshal et al., 2015). Extracellular tau can impact the electrophysiological activity of neurons (Bright et al., 2015; Gómez-Ramos et al., 2006; Gómez-Ramos et al., 2008) and there is evidence that tau oligomers may also have similar effects (Bright et al., 2015; Pá et al., 2016; Gómez-Ramos et al., 2006; Gómez-Ramos et al., 2008; Hill et al., 2019).

In tauopathies, tau is transformed by an unknown trigger to adopt a pathogenic structure and to assemble into oligomeric or fibrillar aggregates that can drive misfolding of nonpathological tau (Fuster-Matanzo et al., 2018; Wang and Mandelkow, 2016; Yamada, 2017). Although templated misfolding occurs intracellularly, some of these tau “seeds” may be released into the extracellular space and internalized by neighboring cells where they can seed intracellular tau aggregation. In this self-perpetuating process, seeded aggregation of conformationally altered tau may spread along neuronal networks to interconnected neurons and adjacent glial cells from one neuroanatomically connected brain region to another and thus propagate tau pathology (Fuster-Matanzo et al., 2018; Gibbons et al., 2019; Wang and Mandelkow, 2016; Yamada, 2017). The hypothesis of transcellular tau spreading is supported by data showing that exogenously applied recombinant tau fibrils, tau oligomers or

aggregates present in CSF, or homogenates prepared from the brains of individuals with Alzheimer's disease (AD) can enter cells in culture or *in vivo* and seed tau pathology (Albert et al., 2019; Courade et al., 2018; Guo et al., 2016; Lasagna-Reeves et al., 2012; Mirbaha et al., 2015; Sanders et al., 2014; Skachokova et al., 2019; Takeda et al., 2016; Wang and Mandelkow, 2016). Pathological tau aggregates cause neuronal dysfunction and cell death, which can manifest as neurodegenerative disorders such as AD, progressive supranuclear palsy (PSP), and corticobasal degeneration (CBD) (Guo et al., 2017). As a means to attenuate the transfer of extracellular tau and slow disease progression, a number of tau immunotherapies are under investigation (Colin et al., 2020; Jadhav et al., 2019; Novak et al., 2018; Sigurdsson, 2018).

Gosuranemab (BIIB092) is a humanized IgG_4P monoclonal antibody directed against the N-terminus of tau (Boxer et al., 2019). It was derived from the murine IgG_1 monoclonal antibody IPN002, which binds with high affinity to human tau that possesses its N-terminal epitope, herein referred to as N-terminal tau (Bright et al., 2015). IPN002 was generated by immunization of mice with *in vitro* aggregated 2N4R human tau. It was selected for its high affinity and ability to normalize increased electrophysiological activity in neurons exposed to N-terminal tau fragments (Bright et al., 2015). Repeated administration of gosuranemab has been demonstrated to be well tolerated in healthy volunteers and trial participants with PSP (Boxer et al., 2019; Qureshi et al., 2018). Gosuranemab was previously investigated as a treatment for PSP and the results failed to demonstrate clinical efficacy. It is currently being tested as a therapy for AD (NCT03352557).

Here, we describe in detail the interactions between gosuranemab and tau. We characterized the affinity and functional consequences of gosuranemab–tau binding *in vitro*, including in human CSF and in pathological brain homogenates, as well as in a transgenic mouse model. We compared binding affinities of gosuranemab with those of other clinical anti-tau antibodies, such as tilavonemab, (Yanamandra et al., 2015), zagotenemab, (Jicha et al., 1997), UCB0107 (Courade et al., 2018), and semorinemab (Adolfsson et al., 2018; World Health Organization, 2018). We report the molecular details of antigen binding deduced from the crystal structure of the murine version of the gosuranemab (IPN002) Fab/tau peptide complex. Gosuranemab bound with high affinity to an eight-residue epitope at the N-terminus of tau that is shared among all tau isoforms. Gosuranemab recognized insoluble pathological tau from different tauopathies; the high affinity of gosuranemab for different tau strains may enable it to interfere with the neuronal transmission of seed-competent tau across a broad range of disease states. Gosuranemab inhibited tau seeding activity from brain homogenates and ISF in cell

models and exhibited near-complete target engagement in ISF and CSF.

2. Materials and methods

2.1. Recombinant tau expression and purification

6xHis-tagged human 2N4R tau was overexpressed in BL21 Star (DE3) pLysS bacteria and purified as previously described (Li and Lee, 2006). Briefly, pelleted cells were resuspended on ice in high-salt RAB buffer (0.1 M MES, 1 mM EGTA, 0.5 mM $MgSO_4$, 0.75 M NaCl, 0.02 M NaF, 1 mM phenylmethylsulfonyl fluoride, 0.1% protease inhibitor cocktail [100 µg/mL each of pepstatin A, leupeptin, tosyl phenylalanyl chloromethyl ketone, tosyl-L-lysyl-chloromethane hydrochloride, and soybean trypsin inhibitor, and 100 mM EGTA]; pH 7.0), homogenized, boiled at 100°C for 10 min, and then rapidly cooled on ice for 20 min. After centrifugation at 70,000 g for 30 min, the supernatant was dialyzed into FPLC buffer (20 mM piperazine-N,N'-bis [2-ethanesulfonic acid], 10 mM NaCl, 1 mM EGTA, 1 mM $MgSO_4$, 2 mM dithiothreitol, 0.1 mM phenylmethylsulfonyl fluoride; pH 6.5) and applied to a 5-mL HiTrap SP Sepharose high performance IEX cation-exchange column (GE Healthcare Life Sciences, Chicago, IL). Tau was eluted using a 0 to 400 mM NaCl gradient in FPLC buffer. Peak fractions were pooled and dialyzed into 100 mM sodium acetate pH 7.0 and concentrated to approximately 5 mg/mL using an Amicon spin concentrator (Millipore Corp, Billerica, MA). Final protein concentration was determined using bicinchoninic acid protein assay (Pierce™, Thermo Fisher Scientific, Waltham, MA).

2.2. Preparation of tau fibrils

Tau monomer (purified as described above) was diluted to 40 µM in 100 mM sodium acetate pH 7.0 with 2 mM dithiothreitol and heated for 10 min at 55°C. Low-molecular-weight heparin (Millipore Sigma, USA) was added to a final concentration of 40 µM. The mixture was distributed to a 96-well plate and shaken in a tabletop Thermomixer (Eppendorf, USA) at 37°C and 1000 rpm for 7 days. Insoluble tau was pelleted by ultracentrifugation at 100,000 g for 30 min at 4°C. The pellet was washed twice by vigorous pipetting in 100 mM sodium acetate pH 7.0 and resuspended in the same buffer. Aggregate formation was monitored by sedimentation assay, thioflavin binding assay, and negative stain transmission electron microscopy.

2.3. Pathological tau preparation

Insoluble tau from AD, CBD, and PSP samples was enriched as described previously (Narasimhan

et al., 2017). Areas of extensive tau pathology were identified by immunohistochemical evaluation of paraffin-embedded brain sections utilizing the AT8 antibody, and these brain tissues were used to generate partially purified and concentrated preparations of filamentous tau representative of each tauopathy (Narasimhan et al., 2017). PSP and CBD brain lysates were prepared from a single case with confirmed neuropathological diagnosis; frontal cortical region (grey and white matter together) was used for extractions. AD-tau was prepared from frontal cortex grey matter dissected from three individuals with neuropathological diagnosis and high tau load from histology reports (two preparations were from the same brain). The four separate AD-tau preparations were pooled and characterized (Supplementary Table 1). Samples were derived from the Center for Neurodegenerative Disease brain bank, University of Pennsylvania.

2.4. Tau direct-binding ELISA

Human 2N4R tau (rPeptide, Watkinsville, GA) in phosphate-buffered saline (PBS) was coated at a final concentration of 0.1, 0.25, or 1 µg/mL overnight at 4°C in 96-well plates (Nunc MaxiSorp; Thermo Fisher Scientific). The plates were washed thrice with PBS-T (PBS, 0.05% Tween-20) and blocked with 400 µL casein in PBS (Thermo Fisher Scientific) for 2 h at room temperature. Block solution was then replaced with serially diluted anti-tau hIgG$_1$ antibodies in casein blocking buffer and incubated for 1 h. The plates were washed thrice with PBS-T. Captured antibodies were detected by subsequent incubation for 30 min with donkey anti-human IgG, Fcγ fragment–specific secondary antibody (Jackson ImmunoResearch Laboratories, West Grove, PA) diluted 1:10,000 in casein block. Horseradish peroxidase (HRP) activity was measured by incubation with 1-step Ultra TMB–enzyme-linked immunosorbent assay (ELISA) substrate (Thermo Fisher Scientific). Developed ELISAs were stopped by the addition of 2N H_2SO_4 and plates were scanned at 450 nm using a Molecular Devices SpectraMax M5 microplate reader. Data were normalized and fitted to a sigmoidal dose-response curve by nonlinear regression.

In order to make relative comparisons in these ELISA assays, variable regions were combined with human IgG$_1$ heavy-chain and human κ light-chain constant regions to generate hIgG$_1$/κ versions of all the clinical anti-tau antibodies (gosuranemab, tilavonemab, zagotenemab, UCB0107, and semorinemab. Reported epitopes and references for each antibody are listed in Supplementary Table 2.

2.5. Tau capture ELISA

Anti–human-Fc monoclonal antibody (Jackson ImmunoResearch Laboratories) at 0.1 µg/mL in PBS was coated overnight at 4°C in 96-well plates (Nunc MaxiSorp; Thermo Fisher Scientific). The plates were washed thrice with PBS-T and blocked with 400 µL casein in PBS (Thermo Fisher Scientific) for 1 h at room temperature. Block solution was then replaced with anti-tau $hIgG_1$ antibodies in casein blocking buffer and incubated for 1 h. The plates were washed thrice with PBS-T and then incubated with serially diluted pathological tau, or preformed tau fibrils derived from recombinant purified 6xHis-tagged human 2N4R tau monomer. Captured tau was detected by subsequent incubation for 30 min with 1 µg/mL of biotinylated anti-tau HT7 $muIgG_1$ monoclonal antibody (Thermo Fisher Scientific) followed by incubation with NeutrAvidin-HRP (Thermo Fisher Scientific) at 1 µg/mL for 30 min. HT7 recognizes a mid-region epitope and did not compete for binding with anti-tau antibodies in this study. HRP activity was measured by incubation with 1-step Ultra TMB-ELISA substrate (Thermo Fisher Scientific). Developed ELISAs were stopped by the addition of 2N H_2SO_4 and plates were scanned at 450 nm using a Molecular Devices SpectraMax M5 microplate reader. Data were normalized and fitted to a sigmoidal dose-response curve by nonlinear regression.

In order to make relative comparisons in these ELISA assays, variable regions were combined with human IgG_1 heavy-chain and human κ light-chain constant regions to generate $hIgG_1$/κ versions of the following clinical-stage anti-tau antibodies: gosuranemab, tilavonemab, zagotenemab, UCB0107, and semorinemab.

2.6. Brain homogenate preparation

Brain tissue (motor cortex for PSP and anterior entorhinal cortex for AD) was procured from the University of Miami Brain Endowment Bank. Donor information in provided in Supplementary Fig. 5. The human biological samples supplied by the brain bank were obtained using an informed consent form that approves the use of human biological samples for research purposes. The use of the human biological samples also conforms with requirements specified in the Statement of Work and all other requirements outlined in the agreement between Biogen and University of Miami Brain Endowment Bank.

Tissue was weighed and homogenized in 3× mass/volume of PBS containing protease and phosphatase inhibitors (Thermo Fisher Scientific). Tissue was homogenized using Bead Ruptor (Omni International, Kennesaw, GA) and the homogenates were sonicated thrice with a Covaris sonicator

(Model E220; Covaris, Woburn, MA), using the 50% maximal power setting. After sonication, homogenates were cleared by centrifugation and tau concentration was determined using INNOTEST hTAU Ag ELISA (Fujirebio, Malvern, PA). All samples were diluted to a final concentration of 1 ng/µL of tau in Opti-MEM (Thermo Fisher Scientific) and 10 ng of tau was used for subsequent immunodepletion and tau aggregation studies.

2.7. Immunodepletion studies

Brain homogenates containing 10 ng of tau were mixed with 3-fold serially diluted gosuranemab, tilavonemab, UCB0107 (final concentrations of 0.00005–1 µg/mL), or control antibody (IgG) in 150 µL of Opti-MEM (ThermoFisher Scientific) containing protease inhibitors (Sigma-Aldrich, Billenica, MA) and allowed to incubate overnight at 4°C. The next day, 50 µL of protein A/G magnetic bead slurry (Thermo Fisher Scientific) was added to each sample to isolate immune complexes. Each immunodepletion reaction was performed in triplicate. Immunodepleted supernatant was transfected into HEK293T tau biosensor cells and tau aggregation was monitored (see below and section 2.8).

For immunodepletion studies with ISF from 11-month-old rTg4510-naïve mice (mouse model of tauopathy, see sections 2.9 and 2.10), ISF from 10 mice was pooled and divided equally for an equivalent volume for each *ex vivo* treatment group. The concentration of tau in ISF from mice of this age was determined to be approximately 30 ng/mL [mid-region tau measured using the Human Total Tau 2.0 immunoassay kit (Quanterix, Billerica, MA) and run on a SIMOA HD-1 analyzer; Supplementary Table 3]. As per the manufacturer's instructions, 30 µg of gosuranemab or control antibody (IgG) was coupled to 1 mg of magnetic M-270 Epoxy beads (Dynabeads Antibody coupling kit; Thermo Fisher Scientific). On the basis of tau seeding experiments with AD brain (described in the Results, section 3.3.1), 3 µg of gosuranemab immunodepletes all seed-competent tau from homogenates containing 10 ng of tau (mid-region measured by INNOTEST), i.e. 1 µg of gosuranemab for 3 ng of tau. The molar concentration of gosuranemab and tau in this assay were 140 nM and 1.3 nM, respectively. On the basis of the concentration of tau in mouse ISF (10.8 ng tau in 360 µL ISF), 0.2 mg of gosuranemab-coupled beads (6 µg antibody if 100% coupling) was used for immunodepletion (2-fold excess compared to that required for complete capture in AD brain homogenate seeding experiments, to accommodate for inefficiency of coupling and ensure complete immunodepletion by gosuranemab given the limited amount of ISF). The molar concentration of gosuranemab and tau in this assay were 114 nM (assuming 100% coupling) and 0.6 nM, respectively. The antibody-conjugated beads, or beads alone, were washed,

blocked with 0.1% bovine serum albumin (BSA) and incubated with ISF overnight. After bead isolation using a magnet, the supernatant (unbound material) was used directly for transfection of HEK293T tau biosensor cells (see section 2.8).

2.8. Tau seeding assay in HEK293T biosensor cells

The HEK293T tau biosensor cell line (HEK293T tau RD-CFP/YFP) (Crotti et al., 2019) was generated similarly to that previously described (Holmes et al., 2014). The cells stably express the repeat domains (RD) of tau protein with a P301S mutation fused to either CFP or YFP. Tau aggregation was measured by CFP to YFP fluorescence resonance energy transfer (FRET) signal, detected with fluorescence-activated cell sorting (FACS).

HEK293T tau biosensor cells were plated in 96-well poly-D-lysine–coated plates at 20,000 cells per well. Immunodepleted ISF (~200 μL) was preincubated with Lipofectamine 2000 (Thermo Fisher Scientific) at a final concentration of 1.25% for 10 min, and ISF-Lipofectamine complexes were added to cells after aspiration of growth media. Cells were incubated for 1 h at 37°C, after which ISF was replaced with complete growth media. Cells were cultured for another 48 h, trypsinized, fixed, and subjected to FRET analysis of tau aggregation by FACS. Aggregation was evaluated using a CFP-YFP FRET pair. Signals were measured on an LSR II flow cytometer (BD Biosciences, San Jose, CA). Forward scatter signal generated by a 488-nm laser line was used as trigger signal. CFP was excited at 407 nm and fluorescence detected with a 450/50-nm bandpass filter indicated no aggregation. YFP excited by CFP emission (FRET) indicated aggregation. The YFP signal was detected using a 505-nm longpass dichroic filter and a 525/50-nm bandpass filter. Samples were acquired using a High Throughput Sampler (HTS or autosampler; BD Biosciences) and FCS 3.0 files were analyzed using FlowJo (BD Biosciences). Data were reported as integrated FRET density, which was calculated as previously described (Holmes et al., 2014):

Integrated FRET density = number of FRET-positive cells × mean FRET signal intensity

For brain homogenates, immunodepleted material (~200 μL) was added directly to the cells after media aspiration, followed by the addition of Lipofectamine 2000 to a final concentration of 1.25%. After 2 h, brain homogenates were replaced with complete growth media and FACS analysis was performed 96 h later.

2.9. Tau assay in ISF and CSF of rTg4510 mice

In the rTg4510 mouse model, constitutive expression of mutant human tau results in the age-

dependent formation of neurofibrillary tangle pathology (Gamache et al., 2019; Ramsden et al., 2005; Santacruz et al., 2005). Four-month-old female rTg4510 mice (strain 129FVB:TgCamk2a-tTA Tg tetO-MAPT*301L; Jackson Laboratory, Bar Harbor, ME) were dosed intraperitoneally with 60 mg/kg of IPN002 or murine IgG_1 isotype control antibody. Mice were dosed weekly for 8 weeks with IPN002 (murine IgG_1 isotype) to avoid an immune response and anti-drug antibody generation that would be evoked with dosing of a human antibody. This isotype is the most inert murine isotype (analogous to $hIgG_4P$ in human) with respect to complement activation and FcR binding (effector function). Seven days after the final dose, microdialysis probes were implanted and ISF sample collection was performed (see details on ISF collection in section 2.10). CSF was collected at this time by terminal draws from the cisterna magna and placed in individual preweighed 0.5 mL tubes. Plasma was collected prior to each antibody administration and at terminal draw; whole blood was collected via the tail vein into EDTA anticoagulant tubes, centrifuged within 1 h of collection, and aliquoted into a 1.5 mL Eppendorf tube. Dosing and collection of ISF and CSF were performed at Charles Rivers Laboratories (San Francisco, CA). ISF and CSF were analyzed for concentrations of unbound N-terminal tau and mid-region tau (Supplementary Fig. 1) using the Human Total Tau 2.0 immunoassay kit (Quanterix, Billerica, MA) and were run on a SIMOA HD-1 analyzer. The detector antibody (ADX215) provided in the tau 2.0 kit has been tested and determined to compete with the binding epitope of gosuranemab; therefore, only unbound N-terminal tau was accessible and measured in this assay. For the unbound N-terminal tau assay, supernatant was diluted 1:4 in diluent provided in the assay kit. For the mid-region tau assay, the detector antibody was 6C5 (Nobuhara et al., 2017), an antibody with a mid-region binding epitope (residues 122–130), and supernatant was diluted 1:2. The mid-region tau assay measures tau levels independent of bound or unbound gosuranemab.

2.10. Microdialysis procedure

Surgical implantation of push-pull microdialysis probes was performed 6 days after the final dose of antibody. Mice were anesthetized using isoflurane (2%, 800 mL/min O_2). Push-pull microdialysis probes (1000 kDa, PE membrane; Brainlink, Groningen, Netherlands) were inserted into the hippocampus. Microdialysis sampling was initiated approximately 24 h after surgery. On the day of the experiment, the probes were connected by fluorinated ethylene propylene tubing to a micro-perfusion pump (Harvard PHD 2000 Syringe pump; Harvard Apparatus, Holliston, MA). Microdialysis probes were perfused with artificial CSF (147 mM NaCl, 3.0 mM KCl, 1.2 mM $CaCl_2$, 1.2 mM $MgCl_2$, 0.15% BSA) at a

flow rate of 0.75 µL/min. Microdialysis samples were collected for 60-min periods directly into 0.5 mL polypropylene Lo-bind tubes (Thermo Fisher Scientific) for 4 h.

For *ex vivo* experiments with ISF from 11-month-old naïve rTg4510 animals for the purpose of evaluating the ability of gosuranemab to immunodeplete seed-competent tau, microdialysis probes were implanted 24 h prior to ISF collection as outlined above.

2.11. Human CSF immunodepletion assay

Human CSF was incubated with gosuranemab or isotype control (human IgG_1) antibody, and the resulting immune complexes were removed using protein A/G magnetic beads. The immunodepleted supernatant was assayed for unbound N-terminal tau. CSF from 3 healthy volunteers (HVs) was combined into one pool (HV pool), CSF from 4 individuals with AD into a second pool (AD pool), and CSF from 4 individuals with PSP into a third pool (PSP pool). Detail donor information is provided in Supplementary Table 5. Each pool was split into 10 equal-volume aliquots. Gosuranemab was added at a top concentration of 20 µg/mL, and serially diluted 10-fold for a total of 8 aliquots. Isotype control antibody was added to an additional aliquot at a final concentration of 20 µg/mL (approximately 150 nM). A final aliquot was used as a no-antibody control. All aliquots were incubated overnight at 4°C with rotation. For removal of gosuranemab–tau complexes, 1.5 mg of protein A/G magnetic beads (Pierce) were added to each aliquot, and tubes incubated for 45 min at 4°C with rotation. All tubes were then placed on a magnet for 1 min, and supernatant collected. Supernatant samples were analyzed on the same day. The limit of detection for the unbound N-terminal tau and mid-region tau assays were 0.1 pg/mL and 7.8 pg/mL, respectively.

2.12. Tau seeding assay in mouse primary cortical neurons

Primary cortical neurons were prepared from embryonic E16-18 CD1 mice (Charles River) in 96-well plates at 17,500 cells per well. After 7 days *in vitro*, primary mouse neurons were treated with 1, 2, 4, and 8 µg/mL gosuranemab (6.7, 13.3, 26.7, and 53.3 nM, respectively), 4 µg/mL Tau5, or 8 µg/mL control IgG, followed immediately by the addition of 125 ng (30.3 nM) of paired helical filament tau, purified from AD brain as previously described (Guo et al., 2016; Narasimhan et al., 2017); the molar ratios were approximately 1:5, 1:2, 1:1, and 2:1, antibody:PHF tau. Tau aggregates were allowed to develop for an additional 2 weeks; on day 21, soluble mouse tau was extracted with 1% Hexadecyltrimethylammonium bromide (HDTA) for 15 min at 22°C and cells were then fixed with 4%

paraformaldehyde, 4% sucrose in PBS for 15 min at 22°C (Crowe et al., 2020). Tau pathology was stained using anti–mouse tau rabbit polyclonal antibody R2295 (Guo et al., 2016). Tau aggregates were imaged by fluorescence microscopy using an IN Cell Analyzer 2200 (GE Healthcare Life Sciences) and quantified with IN Cell Developer Toolbox software. The density and area of insoluble mouse tau was assessed in six regions of each well, and the density × area was normalized to the number of DAPI-positive nuclei. The experiment was performed in triplicate, with three independent wells per condition.

2.13. Surface plasmon resonance

The affinity of anti-tau antibodies for tau was confirmed using surface plasmon resonance to measure the monovalent binding affinity of Fab fragments. Human 0N4R tau was biotinylated using KPL SureLINK^{TM} Chromophoric Biotin (Seracare Life Sciences, Milford, MA) as per instruction in the manufacturer's manual. Binding kinetics and affinity analysis were performed on a Biacore T200 with a biotin capture chip and reagents (GE Healthcare Life Sciences), in binding buffer (10 mM HEPES, 150 mM NaCl, 3 mM EDTA, 0.005% surfactant P20, 0.05% BSA; pH 7). Biotin tau was immobilized on a biotin capture sensor chip at 10–50 pg/mm^2. Dilutions of anti-tau antibody Fab fragments were injected for 5 min and then washed out to monitor dissociation for 15 min, at a 30 µL/min flow rate. The chip was regenerated to remove biotin-captured tau after each measurement with a 2-min injection of 6 M guanidine, 0.25 M NaOH. Data were analyzed with BIAevaluation 3.0 software (Biacore, Uppsala, Sweden). The association and dissociation rate constants were determined from fits of the data to a 1:1 kinetic binding model, or equilibrium dissociation constants were fit from steady-state binding levels (for zagotenemab). Fab fragments used for these experiments were generated by papain cleavage of human IgG_1/κ versions of clinical anti-tau antibodies. Mass spectrometry was used to confirm purity of Fab preparation.

2.14. X-ray crystallography

The IPN002 Fab/tau peptide complex was prepared by mixing the IPN002 Fab fragment at 10 mg/mL with a 5-fold molar excess of $tau_{9–26}$ peptide (EVMEDHAGTYGLGDRKDQ; GenScript, Piscataway, NJ) in 25 mM HEPES pH 7.5, 100 mM NaCl. Crystallization was performed by the nanodroplet vapor diffusion method at 4°C by mixing 200 nL of the complex with 200 nL of the reservoir solution, which contained 100 mM Tris hydrochloride pH 8.5, 20% w/v polyethylene glycol 2000 monomethyl ether, 200 mM trimethylamine N-oxide as precipitant, and 100 mM non-detergent

sulfobetaine 201 as an additive. Crystals grew to full size (200 µm × 100 µm × 100 µm) in 1 week. The crystals were harvested under an oil-based cryoprotectant (66.5% [w/w] Paratone-N, 28.5% [v/v] paraffin oil, and 5% [v/v] glycerol) (Sugahara and Kunishima, 2006) and were flash-frozen in liquid nitrogen.

Diffraction data were collected at beamline 31-ID of Advanced Photon Source at −173°C using a Pilatus3 S 6M detector and processed in the monoclinic space group P1 using the program XDS (Kabsch, 2010). Data were integrated, reduced, and scaled using XDS in the monoclinic space group P1. The structure of the IPN002 Fab/tau complex was determined to 1.56 Å resolution by molecular replacement using the program Phaser (McCoy et al., 2007) in the CCP4 suite (Winn et al., 2011), using a previously published structure (PDB accession number 5B6F) as the search model. Residues 15–22 of the tau peptide were manually built into the F_o-F_c electron density map using Coot (Emsley et al., 2010) and the model was further refined using Phenix (Adams et al., 2010). The progress of the model refinement was monitored by cross-validation R_{free}, which was computed from a randomly assigned test set comprising 5% of the data. The final model includes one Fab molecule, one $tau_{15–22}$ peptide, and 394 water molecules in the asymmetric unit. The final R factor is 22.8% with a R_{free} factor of 26.8%. Atomic coordinates and experimental structure factors of the IPN002 Fab/tau_{15-22} complex have been deposited in the Protein Data Bank with the accession number 6PXR. Figures were prepared with PyMOL (Schrödinger Inc., New York, NY). The interface area and the buried ratio were calculated using CCP4 programs PISA and AreaiMol (Krissinel and Henrick, 2007; Lee and Richards, 1971). Shape complementarity between IPN002 and tau was calculated with S_c (Lawrence and Colman, 1993). The number of interface atoms was calculated using CCP4 program Ncont with maximum distance at 4.0 Å.

2.15. Microscale thermophoresis

Microscale thermophoresis (MST)-binding studies with IPN002 and tau peptides (GenScript) were performed with a Monolith NT.115 instrument (NanoTemper Technologies Inc., San Francisco, CA). NHS ester–coupled fluorescent dye (NanoTemper Technologies Inc.) was used to label IPN002, and the temperature-induced change in fluorescence was detected as a function of the concentration of tau peptides. The LED power was set at 95%, at which power the fluorescence counts were approximately 1000 units for all samples. The samples were loaded into capillaries coated with a hydrophobic layer. Fluorescence was measured for 5 s, after which thermophoresis was started. Samples were heated for 45 s at 70% laser power, followed by 5 s of cooling. All experiments were replicated three times. The

average value of normalized fluorescence (F_{norm} = fluorescence intensity after thermophoresis/fluorescence intensity before thermophoresis) was plotted against the peptide concentration, and the curves were analyzed using NanoTemper analysis software (Version 1.5.35; NanoTemper Technologies, Inc.) to calculate the dissociation constant (K_D) values.

2.16. Capture ELISA to measure antibody levels in mouse plasma

Human 0N4R tau (rPeptide, Watkinsville, GA), at 1 μg/mL in PBS, was coated overnight at 4°C in 96-well plates (Nunc MaxiSorp; Thermo Fisher Scientific). The plates were washed four times with PBS-T and blocked with 300 μL of 1% casein in PBS (Thermo Fisher Scientific) for ≥1 h. Standard curve samples of IPN002 were generated by spiking IPN002 into diluted blocking buffer (0.1% filtered casein in PBS) in a concentration series starting at 10 μg/mL, preceded by eleven 3-fold serial dilutions and including buffer-only blank wells. Block was replaced with 50 μL per well of sample diluted 1:20,000 in 0.1% filtered casein in PBS, or standard curve samples. Plates were incubated for 1 h at room temperature and washed four times with PBS-T. Goat anti-mouse IgG (heavy-chain residues + light-chain residues) HRP (Jackson ImmunoResearch Laboratories) diluted 1:5000 in 0.1% filtered casein in PBS was added and incubated for 1 h at room temperature (100 μL per well). Plates were washed thrice with PBS-T, incubated for 5 min with 100 μL per well of TMB-ELISA substrate (Thermo Fisher Scientific), followed by 100 μL per well of 2N H_2SO_4 to stop the reaction. Plates were then scanned at 450 nm using a SpectraMax microplate reader (Molecular Devices LLC, San Jose, CA) and data analyzed using SoftMax Pro Software (5-parameter curve fit, Molecular Devices LLC).

3. Results

3.1. Binding properties of gosuranemab anti-tau antibody

3.1.1. Gosuranemab binds tau monomer with high affinity

Gosuranemab was generated by humanizing the variable domains of the murine parent antibody IPN002, and cloning for expression as a human IgG_4 heavy chain, containing the hinge-stabilizing mutation S241P (Kabat numbering), with a human κ light chain. Surface plasmon resonance was used to confirm that gosuranemab retained the same high affinity for human 0N4R tau monomer as the IPN002 parent antibody. Association and dissociation rate constants for gosuranemab were determined from data fit to a 1:1 kinetic binding model (Fig. 1A, red curves), as $k_a = 1.1 \times 10^6\ M^{-1}s^{-1}$ and $k_d = 2.7 \times 10^{-4}\ s^{-1}$, respectively. On the basis of these numbers, the equilibrium dissociation constant, or

monovalent binding affinity for gosuranemab, was estimated to be 0.3 nM (K_D ± standard deviation = 0.3 ± 0.1 nM; Fig. 1A). A similar affinity for human 0N4R tau was measured for IPN002 (K_D = 0.2 nM; Supplementary Fig. 2). Monovalent binding affinities for other anti-tau antibodies (tilavonemab, zagotenemab, UCB0107, and semorinemab) measured using the same assay platform were weaker and estimated to be 13 nM, 260 nM, 85 nM, and 1.4 nM, respectively (Table 1 and Supplementary Fig. 3). These monovalent affinities are generally consistent with previously reported bivalent affinities despite differences in tau monomer coupling strategies (Supplementary Table 1).

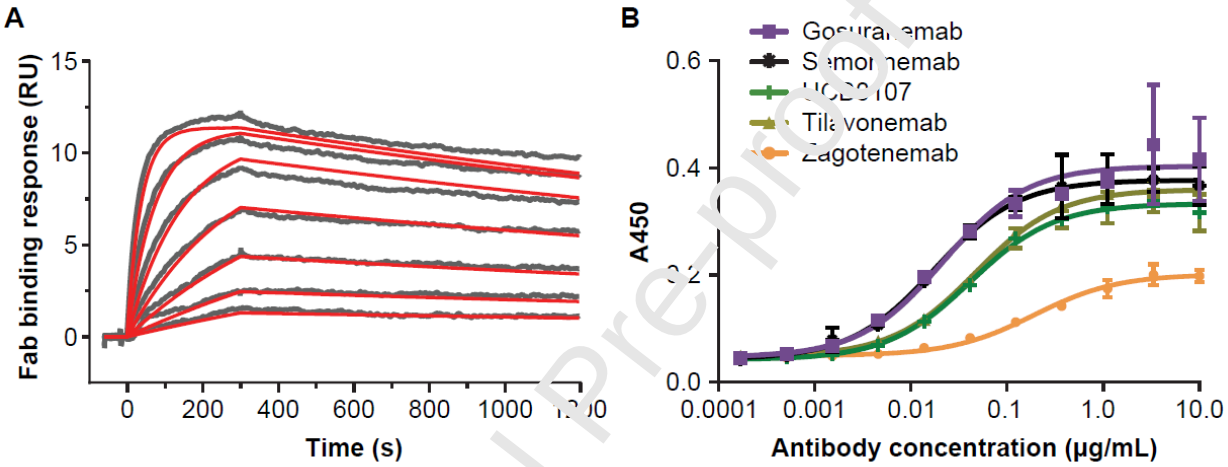

Fig 1. Characterization of tau binding by gosuranemab. (A) Sensorgrams depicting results of surface plasmon resonance analysis of the monovalent affinity and kinetics of gosuranemab Fab binding to human tau isoform 0N4R. Dilutions of gosuranemab Fab at 0.39, 0.78, 1.56, 3.125, 6.25, 12.5 and 25 nM (gray curves) were tested. The association and dissociation rate constants were determined from fits of the data to a 1:1 kinetic binding model (red curves). (B) Graphical depiction of the results of direct tau-binding ELISA for bivalent anti-tau monoclonal antibodies. The graph shows the titration curve for tau monomer binding by antibodies. Detection was at 450 nm with horseradish peroxidase–conjugated anti-human IgG. Error bars represent standard deviation from triplicate measurements (Supplementary Table 4). RU, response units.

To compare intact antibodies for binding mono-dispersed tau, we performed a binding ELISA with recombinant tau monomer coated at low density and bivalent versions of the clinical antibodies tested by surface plasmon resonance. Similar to that previously reported for IPN002 (Bright et al., 2015), the derived half maximal effective concentration (EC_{50}) value for gosuranemab binding to plate-bound recombinant tau monomer was approximately 0.15 nM (Fig. 1B), independent of coating density. Similar subnanomolar EC_{50} values were determined for tilavonemab, UCB0107, and semorinemab despite their lower monovalent affinities, indicating that valency plays a role in this format (Table 1).

	EC_{50} derived from ELISA (nM)	Monovalent affinity (K_D) derived from SPR (nM)
Gosuranemab	0.15	0.3
Tilavonemab	0.32	13
Zagotenemab	1.3	260
UCB0107	0.29	85
Semorinemab	0.12	1.4

Table 1
Affinities of anti-tau antibodies for monomeric recombinant tau derived from either direct-binding ELISA with bivalent monoclonal antibody, or SPR with monovalent Fab fragment.
EC_{50}, half maximal effective concentration.

3.1.2. Gosuranemab binds pathological tau with high affinity

A number of clinical-stage anti-tau antibodies have been shown to recognize pathological aggregated forms of tau (Courade et al., 2018; Gibbons et al., 2018). To understand the biological activity of gosuranemab, and whether gosuranemab can recognize forms of pathological tau that would be characteristic of extracellular "tau seeds," we immobilized gosuranemab and other anti-tau antibodies in order to capture recombinant fibrillar 2N4R tau or diseased tissue-derived tau and measure associations in solution. The EC_{50} value for recombinant tau PFF binding to gosuranemab in this capture format was 5 nM (Fig. 2A; Table 2). Similar EC_{50} values (3–5 nM) were observed for each of the other anti-tau antibodies. These apparent affinities can only be interpreted in relative terms because each fibril likely interacts with multiple antibodies, and many of the tau molecules in a bound fibril will not participate directly in binding. Binding of gosuranemab to tau isolated from diseased brain tissue of

individuals diagnosed with AD, CBD, or PSP was also examined using the tau capture ELISA. The EC_{50} values for binding of gosuranemab to AD-tau, CBD-tau and PSP-tau were determined to be 3 nM, 8 nM, and 3 nM, respectively (Fig. 2B–D; Table 2). Although gosuranemab exhibited similar affinities for tau from each disease, other anti-tau antibodies, i.e. tilavonemab and UCB0107, showed markedly weaker affinities for tau from individuals with CBD relative to that from individuals with AD (Fig. 2B–D; Table 2).

EC_{50} (nM)	Tau PFF	AD-tau	CBD-tau	PSP-tau
Gosuranemab	5	3	8	3
Tilavonemab	4	7	25	12
Zagotenemab	3	6	11	4
UCB0107	4	5	38	NT
Semorinemab	5	3	7	NT

Table 2
Apparent affinities of anti-tau antibodies for pathological tau derived by capture ELISA.
AD, Alzheimer's disease; CBD, corticobasal degeneration; EC_{50}, half maximal effective concentration; NT, not tested; PFF, preformed fibril; PSP, progressive supranuclear palsy.

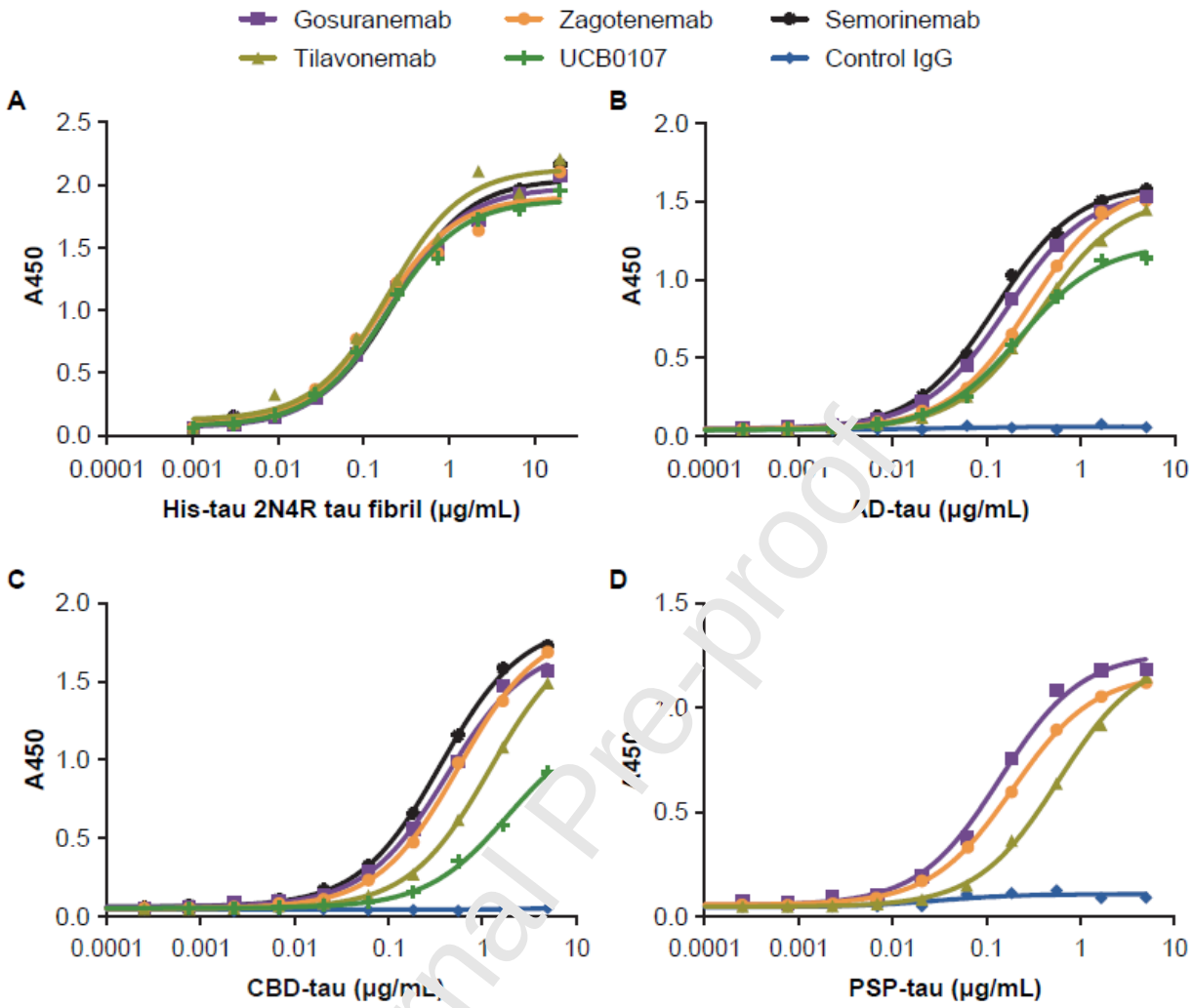

Fig 2. Characterization of pathological tau binding by gosuranemab. Graphical depictions of titration curves from tau capture ELISA for anti-tau antibody binding to (A) full-length recombinant human 2N/4R tau fibrils, (B) AD-tau, (C) CBD-tau, (D) PSP-tau. Detection was at 450 nm with NeutrAvidin-horseradish peroxidase. Standard error was equal to or less than 0.07 µg/mL, 0.02 µg/mL, 0.04 µg/mL, and 0.03 µg/mL for each antibody in experiments with fibrils AD-tau, CBD-tau and PSP-tau, respectively. AD, Alzheimer's disease; CBD, corticobasal degeneration; PSP, progressive supranuclear palsy.

3.2. Structure of gosuranemab in complex with tau

To better understand the structural basis for the high affinity of gosuranemab, we determined the crystal structure of the IPN002 Fab in complex with human tau peptide at 1.6 Å resolution (Fig. 3A). $Tau_{9–26}$ peptide was used for crystallization in order to encompass residues 15–24 that were previously reported to be involved in IPN002 binding (Bright et al., 2015). The statistics of crystallographic data are summarized in Table 3. Only residues 15–22, however, were observed to have well-defined electron density as shown in the composite omit map (Fig. 3B). The lack of electron density for the flanking residues on the N and C termini suggests that these regions of the peptide are disordered and do not interact with the antibody (Fig. 3B). The tau peptide has a type I β-turn formed by residues 16–19, with one hydrogen bond formed between the carbonyl oxygen of G16 and the amide nitrogen of G19, which is further stabilized by one additional hydrogen bond formed between A15 and G21. The key interactions with the tau peptide are formed exclusively through the complementarity-determining regions (CDRs) of IPN002, with the major specificity-determining contacts contributed by CDRs 2 and 3 of the heavy chain (*H*2, *H*3) and CDR 3 of the light chain (*L*3), and a minor contribution by *H*1, *L*1, and *L*2 (Fig. 3C; Table 4).

	Statistic
Data collection	
Space group	P1
Cell dimensions a, b, c (Å), α (°), β (°), γ (°)	42.7, 49.0, 58.7, 85.3, 83.1, 70.7
Resolution (Å)	24.7–1.56 (1.61–1.56)[a]
Rmerge (%)	5.9 (63.8)[a]
I/σ(I)	7.1 (1.3)[a]
CC1/2	0.99 (0.52)[a]
Completeness (%)	95.8 (94.4)[a]
Redundancy	2.0 (2.0)[a]
Refinement[b]	
Number of unique reflections	61,205 (6045)[a]
Rwork/Rfree	0.228/0.268
Number of residues	438
Number of waters	294
RMSD bond lengths (Å)	0.005
RMSD bond angles (°)	0.89
B-factors (Å2)	16.8
Ramachandran regions (%) favored/allowed/disallowed	98/2/0

Table 3
Crystallographic data collection and refinement statistics for IPN002 Fab-tau$_{15–22}$ complex.
[a] Values in parenthesis are for highest resolution shell.
[b] TLS groups were used in the refinement.
RMSD, root-mean-square deviation; TLS, translation/libration/screw.

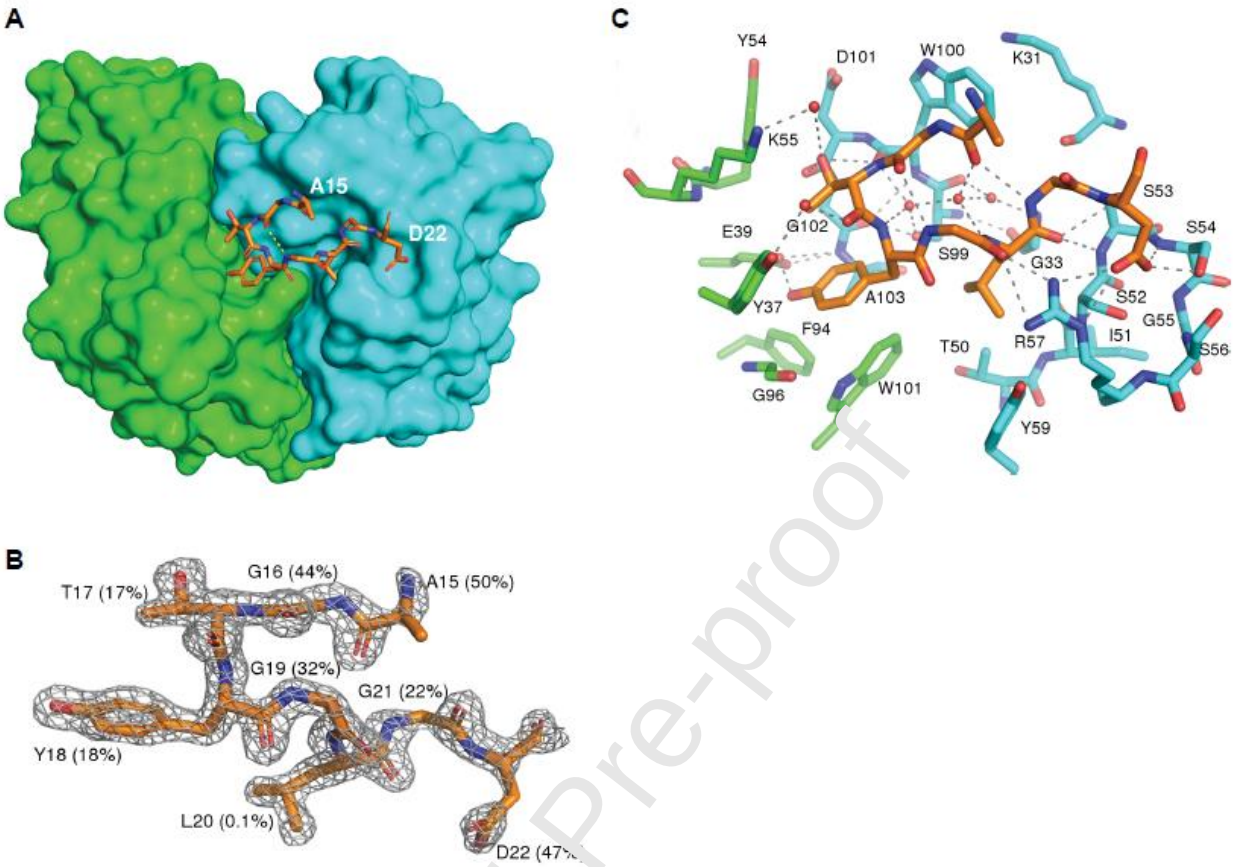

Fig. 3. Crystal structure of IPN002 Fab with tau. Heavy chain of IPN002 is displayed in cyan, light chain in green, and tau peptide in orange. (A) Top view of the IPN002 Fab in surface representation looking down onto the binding paratope. Terminal residues of tau peptide are labeled. (B) Tau peptide conformation when bound to IPN002 Fab from the structure, superposed with an omit electron density map contoured at 3.0σ, shown as mesh. In parentheses is the percentage surface accessibility for each residue, indicating that tau residues 15–22 are mostly buried at the binding surface. (C) Detailed view of the binding interface with key interface residues of IPN002 within 4 Å of the tau peptide shown and labeled; polar interactions are indicated with dashed lines and interface water molecules shown as red spheres.

Tau residue	IPN002 residue
A15	W100*H*
G16	W100*H*[a]
T17	W100*H*[a], D101*H*[a], Y37*L*, K55*L*
Y18	S99*H*, G102*H*, A103*H*, Y37*L*, E39*L*[a], F94*L*, G96*L*, W101*L*
G19	R57*H*[a]
L20	G33*H*, T50*H*, S52*H*, S53*H*[a], R57*H*, Y59*H*
G21	K31*H*, S53*H*
D22	S52*H*[a], S53*H*[a], S54*H*[a], S56*H*, R57*H*[b]

Table 4
Contacts between IPN002 and tau residues. A distance cut-off of 4.0 Å was used.
[a] Hydrogen bond.
[b] Salt bridge.
L, light-chain residues; *H*, heavy-chain residues.

Some notable structural features of the IPN002–tau interface include the complementary hydrophobic and π-stacking contacts made by the side chains T17 and Y18 of tau that bury into the V*H*/V*L* interface of IPN002, formed by residues G102, A103 of the heavy chain, and Y37, E39, F94, G96, and W101 of the light chain (Fig. 3C). Additionally, the charged side chain D22 of tau is close to the oppositely charged residue R57 of the IPN002 heavy chain, forming a salt bridge. At least eight pairs of hydrogen bonds and numerous water-mediated hydrogen bonds stabilize the tau–IPN002 Fab complex (Table 4), which indicates a strong and stable interface. In total, 201 atoms are involved in the tau–IPN002 contacts. Residues 15–22 of the tau peptide have a total surface area of 916 Å^2, of which ~60% (554 Å^2) is buried at the interface with the IPN002 Fab, with tau residue L20 being almost completely buried (Fig. 3B). The shape complementarity of the IPN002–tau interface is 0.77, which is higher than that of an average antibody–antigen interface (0.7) (Kuroda and Gray, 2016). Collectively, these metrics are consistent with the high-affinity binding observed for gosuranemab.

The importance of the molecular contacts seen between IPN002 and tau was substantiated by alanine-scanning mutagenesis in an MST format, using tau peptides containing single alanine substitutions for residues G16–D22 (Supplementary Fig. 4A; Table 5). IPN002 bound tau$_{15–22}$ or tau$_{15–24}$ peptides with similar micromolar affinities, consistent with the epitope spanning residues 15–22, as shown in the crystal structure (Fig. 3). Alanine substitution of T17 or G21 reduced binding as measured

by MST, whereas altering G16, Y18, G19, L20, or D22 eliminated binding (Table 5). Y18 of the epitope is a known site for posttranslational modifications of tau, such as phosphorylation and nitration (Lee et al., 2004; Miyamoto et al., 2017; Reyes et al., 2012). The crystal structure shows that Y18 is tightly packed at the antibody interface with little room to accommodate these functional groups (Fig. 3C). Tau peptides with phosphorylated (pY18) or nitrated Y18 (nY18) lost their ability to bind the antibody (Supplementary Fig. 4B; Table 5). Taken together, the crystal structure and relevant MST studies confirmed that tau residues 15–22 constitute the epitope of IPN002, and that epitope posttranslational modifications can alter antigen recognition.

Peptide name	Sequence	Affinity by MST (μM)
$Tau_{15–24}$	AGTYGLGDRK	16
$Tau_{15–22}$	AGTYGLGD	8
$Tau_{15–24}$ G16A	AATYGLGDRK	No binding
$Tau_{15–24}$ T17A	AGAYGLGDRK	>70
$Tau_{15–24}$ pT17	AG(pT)YGLGDRK	No binding
$Tau_{15–24}$ Y18A	AGTAGLGDRK	No binding
$Tau_{15–24}$ pY18	AGT(pY)GLGDRK	No binding
$Tau_{15–24}$ nY18	AGT(nY)GLGDRK	No binding
$Tau_{15–24}$ pT17/pY18	AG(pT)(pY)GLGDRK	No binding
$Tau_{15–24}$ G19A	AGTYALGDRK	No binding
$Tau_{15–24}$ L20A	AGTYGAGDRK	No binding
$Tau_{15–24}$ G21A	AGTYGLADRK	>100
$Tau_{15–24}$ D22A	AGTYGLGARK	No binding

Table 5
Binding of IPN002 to tau peptides by MST.
MST, microscale thermophoresis.

3.3. Functional properties of gosuranemab

3.3.1. Gosuranemab immunodepletes seed-competent tau from AD and PSP brain homogenates

To test if gosuranemab can reduce tau aggregation induced by tauopathy-derived tau in biosensor cells, immunodepletion experiments were performed using AD brain homogenates and various concentrations of gosuranemab. AD donors from early and late Braak stages were tested individually for seeding activity and no clear relationship between Braak stage and levels of tau aggregation in HEK293T tau biosensor cells was observed for this small cohort (Supplementary Fig. 5A). AD brain homogenates that had significant seeding activity were tested individually or pooled for subsequent studies (Fig. 4B and Supplementary Fig. 5C and 6). Immunodepletion of AD brain homogenates with gosuranemab resulted in a concentration-dependent reduction in tau aggregation, whereas immunodepletion with a control antibody had no effect (Fig. 4B and Supplementary Fig. 5C and 6). Similar results were observed with individual PSP brain homogenates (Fig. 4C and Supplementary Fig. 5D). Empirical data from clinical trial NCT02460094 showed that serum C_{max} at day 57 for a gosuranemab 2100 mg cohort was 913 µg/mL (Boxer et al., 2019). The gosuranemab CSF:serum ratio was reported to be approximately 0.4% across all doses tested and generally similar between days 29 and 85, and therefore CSF C_{max} was approximately 30 nM. Notably, 2100 mg is the administered dose in our phase 2 study of gosuranemab in participants with AD (TANGO, NCT03352557). Derived IC_{50} values from our brain homogenate seeding experiments ranged from 17–60 pM, well below the observed maximal gosuranemab CSF concentration in the 2100 mg cohort and therefore concentrations used in the brain homogenate seeding assays are therapeutically relevant. We examined the activity of gosuranemab in the AD brain homogenate seeding assay relative to that of other anti-tau antibodies, i.e. tilavonemab and UCB0107. Both tilavonemab and UCB0107 had activity in this functional assay (Supplementary Fig. 6). The observations are consistent, i.e. all antibodies behaved similarly, with data derived from binding experiments carried out using pooled AD brain homogenate from different donors (Fig. 2B and Table 2). Similar functional experiments with CBD and PSP brain homogenates were not performed. These experiments demonstrated that gosuranemab has high affinity for pathological tau seeds from AD- and PSP-diseased brains that induce cellular tau aggregation.

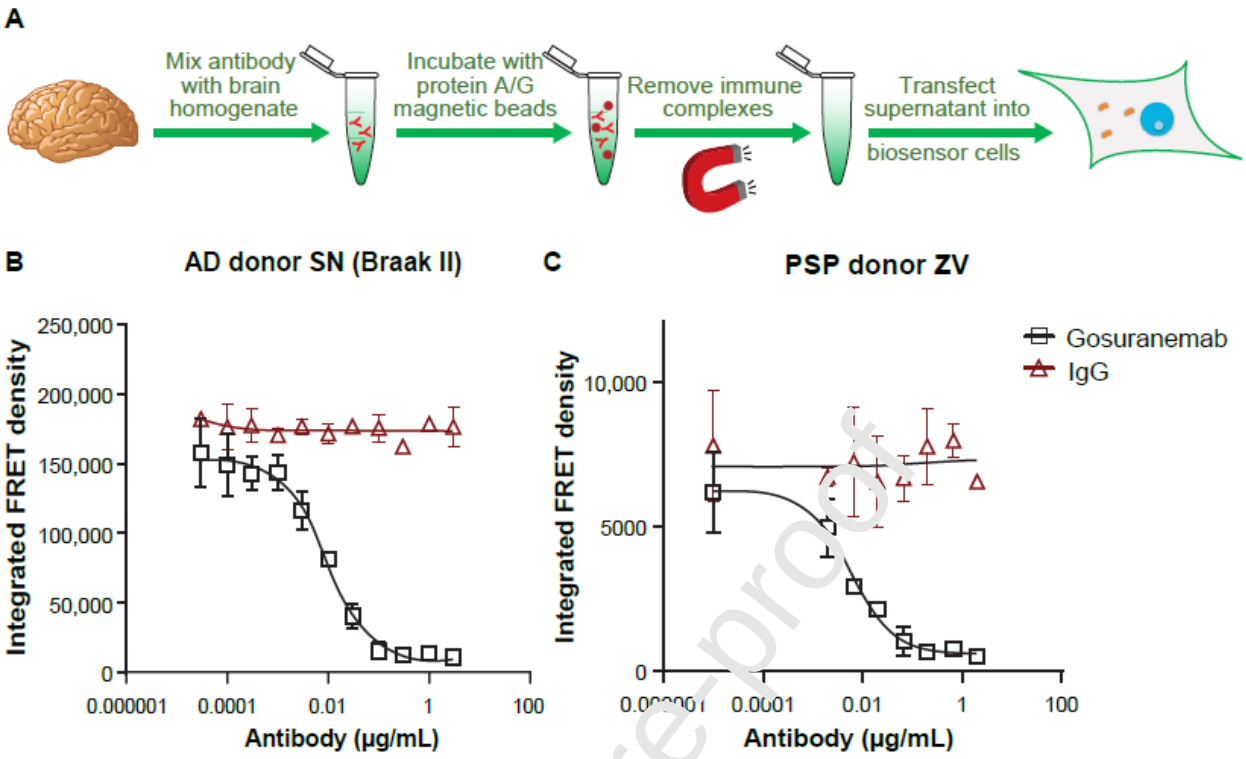

Fig. 4. Gosuranemab immunodepletes seed-competent tau from AD and PSP brain homogenates. (A) Assay schematic. Brain homogenates were incubated with the antibody, after which immune complexes were removed using protein A/G magnetic beads and the supernatants were transfected into HEK293T tau biosensor cells. (B, C) Titration curves of antibodies used for immunodepletion of brain homogenate versus FRET signal from HEK293T tau biosensor cells. Data were fitted to a non-linear regression curve; each antibody concentration was tested in triplicate, error bars represent standard error of the mean. IgG is an isotype control antibody. (B) A single AD donor (donor SN in Supplementary Fig. 5) was used to generate AD brain homogenate. The derived IC_{50} value for gosuranemab from this experiment was approximately 60 pM. (C) A single donor (donor ZV in Supplementary Fig. 5) was used to generate PSP brain homogenate. The derived IC_{50} value for gosuranemab from this specific experiment was approximately 38 pM. See Supplementary Fig. 5C-D for experiments with additional donors. AD, Alzheimer's disease; FRET, fluorescence resonance energy transfer; IC_{50}, half maximal inhibitory concentration; PSP, progressive supranuclear palsy.

3.3.2. Gosuranemab immunodepletes seed-competent tau present in ISF of rTg4510 tauopathy model

To investigate whether gosuranemab can bind seed-competent tau in ISF and reduce tau aggregation induced by ISF in biosensor cells, immunodepletion experiments were performed using ISF from the rTg4510 mouse model (Ramsden et al., 2005; Santacruz et al., 2005). ISF from multiple 11-month-old rTg4510 mice was collected by microdialysis, pooled, and incubated with a concentration of gosuranemab effective at depleting seed-competent tau from AD brain homogenate (Fig. 5A). HEK293T tau biosensor cells were treated with the immunodepleted ISF, and tau aggregation was measured. Naïve ISF exhibited significant tau seeding activity and the control antibody had minimal effect on reducing that activity; however, immunodepletion with gosuranemab reduced ISF seeding activity below the detection level of the assay (Fig. 5B). These results suggest that gosuranemab can interact with extracellular seed-competent tau and has the potential to interrupt tau seeding and spreading *in vivo*.

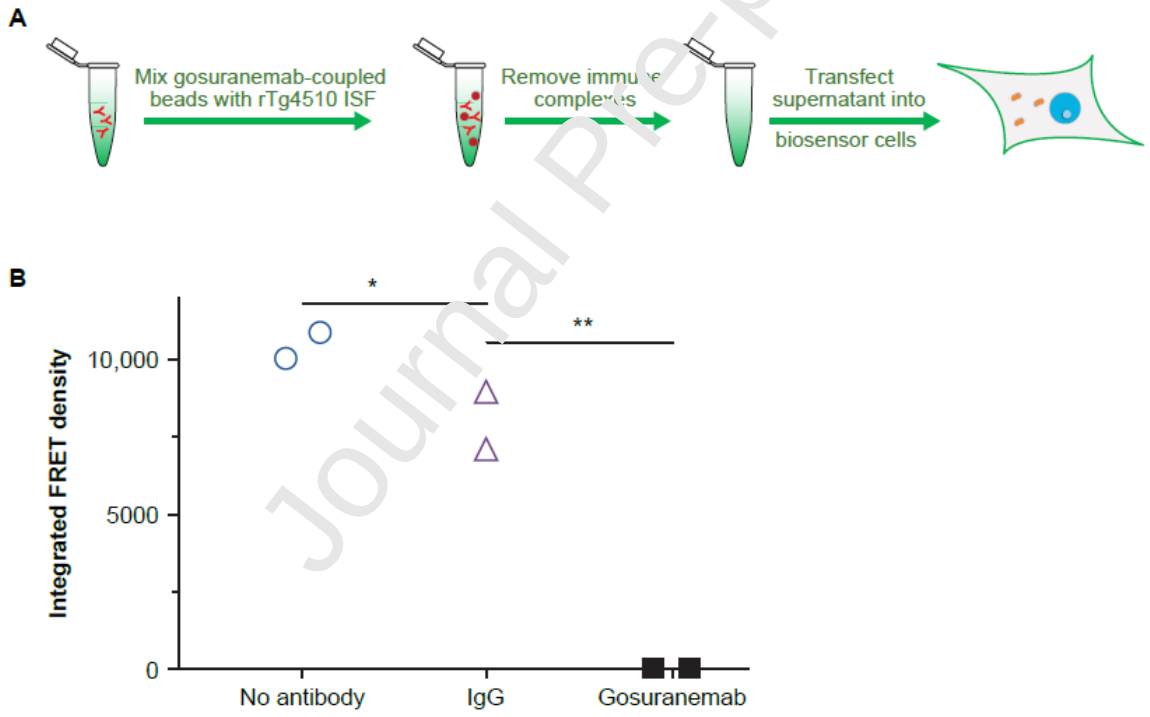

Fig. 5. Gosuranemab immunodepletes seed-competent tau from interstitial fluid (ISF) of rTg4510 mice. (A) Assay schematic. ISF from 11-month-old rTg4510 mice was collected using microdialysis, and was pooled and divided equally between different immunodepletion groups. (B) After immunodepletion, ISF was added to HEK293 tau biosensor cells for tau aggregation induction. Each immunodepletion group was tested in duplicate. Statistical significance assessed by one-way ANOVA (p=0.0022) with Dunnett's multiple comparisons test. *p=0.0961, **p=0.0039. FRET, fluorescence resonance energy transfer.

3.3.3. Gosuranemab prevents tau aggregation in mouse primary cortical neurons

To investigate whether the presence of gosuranemab would interfere with the development of intracellular tau pathology initiated by an extracellular tau seed, and to extend the analysis beyond engineered cultured cells, we treated wildtype mouse primary cortical neurons with human AD-tau enriched from AD brain homogenates, and measured insoluble tau inclusions with high-content cell imaging (Fig. 6A). In the absence of AD-tau treatment, tau aggregation in the cultured mouse neurons was nearly undetectable (Fig. 6B and C). For neurons exposed to AD-tau, there was a significant and robust induction of tau aggregation. Preincubation of AD-tau with gosuranemab resulted in a concentration-dependent reduction in tau aggregation, with the highest concentrations (4 and 8 μg/mL) resulting in a maximum ~50% reduction in aggregation compared with AD-tau alone , which was the maximal inhibition observed in this assay. Preincubation with Tau5 at 4 μg/mL had a similar degree of effect (Fig. 6B).

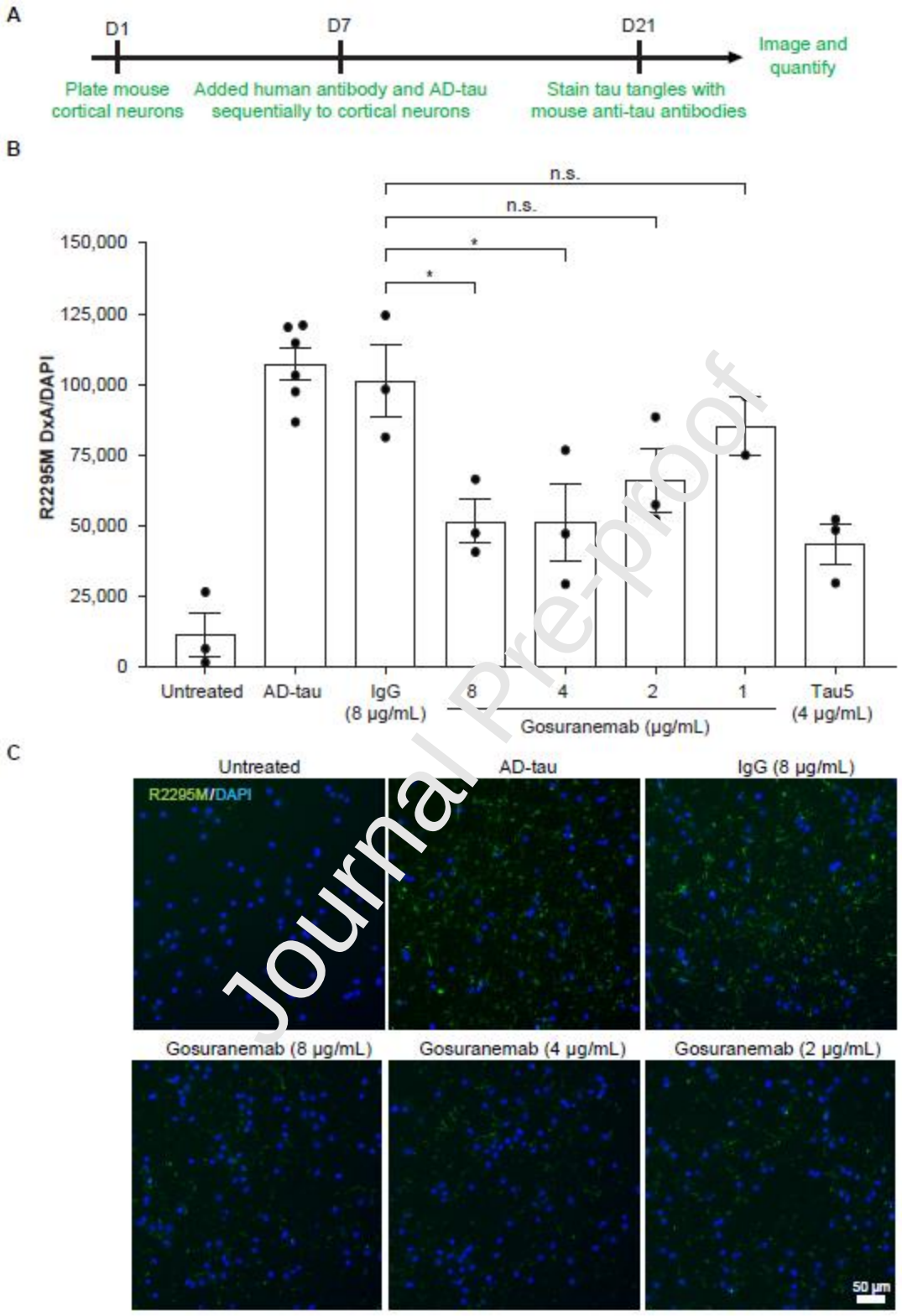

Fig. 6. Gosuranemab blocks tau aggregation induced by AD-tau in primary mouse neurons. (A) Assay timeline. (B) Insoluble tau aggregates, induced by exposure to AD-tau, were stained using the R2295

mouse tau specific anti-tau antibody and quantified: density × area was normalized to the number of DAPI-positive nuclei. Error bars indicate the standard deviation from *n* = 2–3 technical replicates, representative of *n* = 3 biological replicates. Statistical significance assessed by one-way ANOVA with Tukey's multiple comparison post-hoc test. *p<0.05. Estimated IC_{50} for gosuranemab was 2 μg/mL. (C) Immunocytochemistry images of gosuranemab inhibition of AD-tau induced mouse tau pathology in neurons stained with R2295 (green) and DAPI (blue), scale bar 50 μm. AD, Alzheimer's disease; D, day; n.s., not significant.

3.3.4. Gosuranemab binds extracellular tau in rTg4510 model

The ability of IPN002 to bind extracellular tau has been examined previously, using 3.5-month-old JNPL3 P301L transgenic mice and 5.5-month-old tau-4R/2N-P301L (van Leuven) transgenic mice (Bright et al., 2015). Near-complete target engagement was observed in ISF from JNPL3 mice and in CSF from van Leuven mice treated with 60 mg/kg and 20 mg/kg of IPN002, after 8 and 26 weeks of dosing, respectively; IPN002 treatment decreased free human tau by 94% in ISF and by 98% in CSF, compared with IgG control–treated mice. For the purposes of examining the level of target engagement in ISF and CSF in a different model using newly developed, more sensitive assays, and additionally the level of N-terminal and mid-region tau after IPN002 treatment, we carried out a similar experiment in the rTg4510 mouse model (Ramsden et al., 2005; Santacruz et al., 2005). We matched the dose and duration of the JNPL3 study since "free" or unbound N-terminal tau in ISF was not zero for all animals dosed (Bright et al., 2015) and extracellular tau levels (using mid-domain assays) in rTg4510 mice are in the range of 20–40 ng/ml (Sankaranarayanan et al., 2015), three-fold higher than JNPL3 mice. The high levels of extracellular tau observed in rTg4510 mice make it an attractive model for measuring tau target engagement. Notably, tau pathology was not examined in this study given that the highly aggressive nature of tau deposition in this model is presumed to develop in a cell-autonomous manner without extracellular spread. Animals were dosed with IPN002 weekly at 60 mg/kg for 8 weeks (Fig. 7A). IPN002 concentrations in plasma were consistent with predicted exposure [~800 μg/mL (5.5 μM) maintained after 14 days; Supplementary Fig. 6]. Mid-region and unbound N-terminal (i.e. not bound by IPN002) tau in CSF and ISF collected 8 days after the final dose were measured using an ultrasensitive immunoassay (see section 2.8). The concentrations of unbound N-terminal tau in CSF and ISF were reduced to background levels in the IPN002-treated animals, relative to animals treated with the muIgG_1 isotype control antibody (Fig. 7B, $p < 0.001$ for CSF and ISF). Mid-region tau levels in the CSF and ISF showed a trend toward reduction but were not significantly changed in response to IPN002 treatment (Fig. 7C).

The observed reduction of unbound N-terminal tau in CSF and ISF demonstrates that systemically administered gosuranemab sufficiently entered the central nervous system and bound N-terminal extracellular tau.

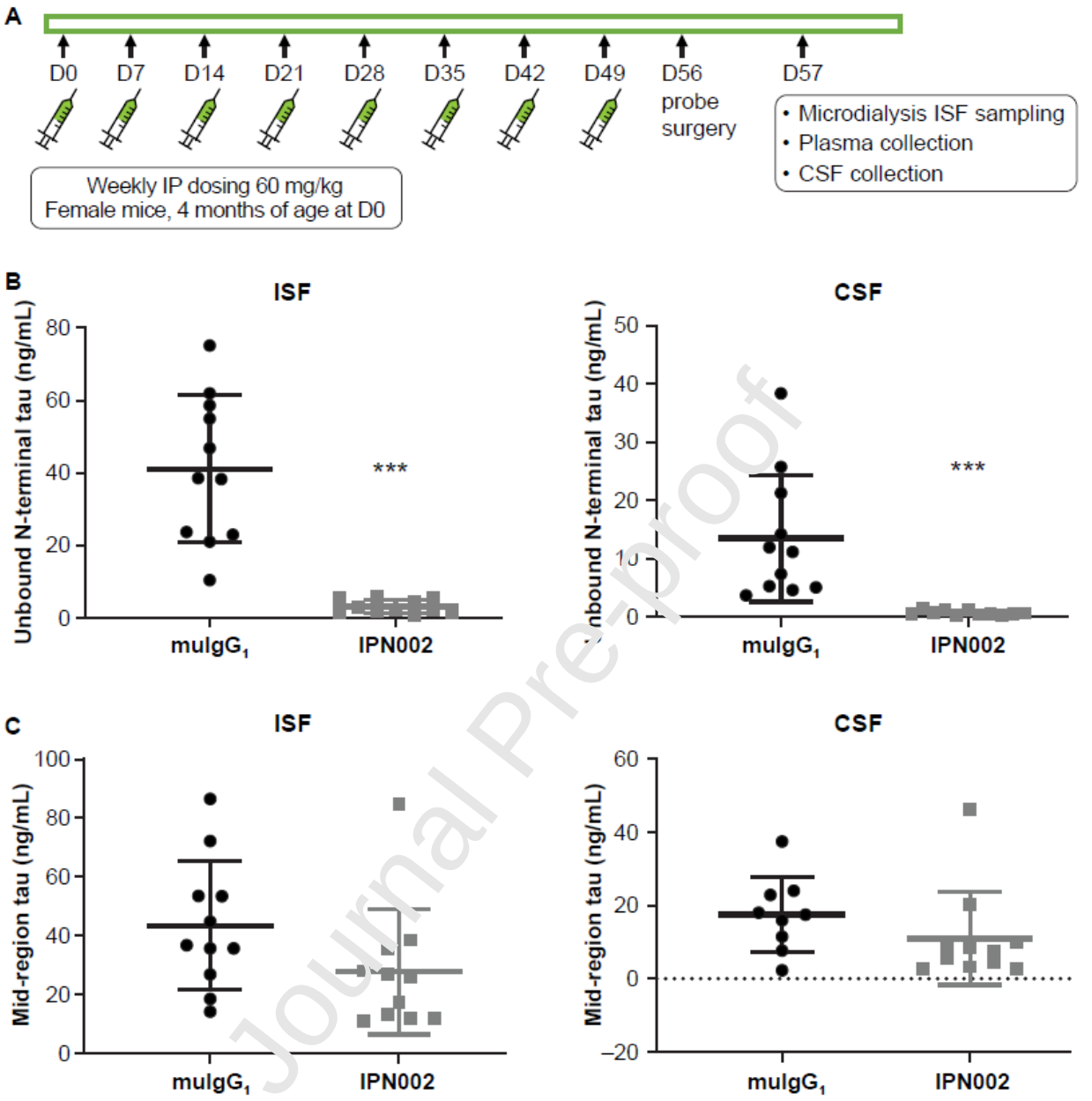

Fig. 7. IPN002 target engagement in rTg4510 mouse model. (A) Study design and dosing regimen using rTg4510 human tau–transgenic mice. (B) Unbound N-terminal tau was significantly reduced in ISF and CSF with IPN002 dosing, compared with treatment with a control antibody (murine IgG_1). (C) Mid-region tau was not significantly reduced in ISF and CSF with IPN002 dosing, compared with dosing with an isotype control antibody. Each data point is representative of one animal in the study. ***$p < 0.001$ (unpaired *t*-test). Error bars represent standard error of the mean. CSF, cerebrospinal fluid; D, day; IP, intraperitoneal; ISF, interstitial fluid.

3.3.5. Gosuranemab binds to tau in PSP and AD CSF

Data from a multiple ascending dose phase 1b study indicated that gosuranemab can bind tau in the CSF of individuals diagnosed with PSP (Boxer et al., 2019). To assess if gosuranemab can also bind to extracellular tau in CSF from individuals diagnosed with AD, an immunodepletion assay evaluating varying concentrations of gosuranemab was conducted in antemortem AD, PSP, and HV CSF (Fig. 8A). The concentration of gosuranemab effective at engaging all N-terminal tau in this assay (150 pM) is 0.5% of the concentration circulating in patient CSF four weeks post administration of 2100 mg gosuranemab (Boxer et al., 2019). After gosuranemab–tau immune complex removal, target engagement was deduced from measuring residual levels of N terminus containing tau. As expected, gosuranemab treatment resulted in a concentration-dependent reduction in N-terminal tau in PSP and HV CSF (Fig. 8 B–C). A similar trend was observed for AD CSF (Fig. 8D). Like PSP CSF, complete target engagement (as demonstrated by the inability to detect N-terminal tau with our ultrasensitive platform) in AD CSF was observed with 150 pM gosuranemab (Fig. 8D). At this concentration, levels of mid-region tau approached 50% of that measured in naive CSF, or CSF immunodepleted using control antibody (Fig. 8E-G). These observations indicate that half of all mid-region tau fragments have an intact N-terminus, and suggest that approximately two thirds of all extracellular tau could be targeted by gosuranemab.

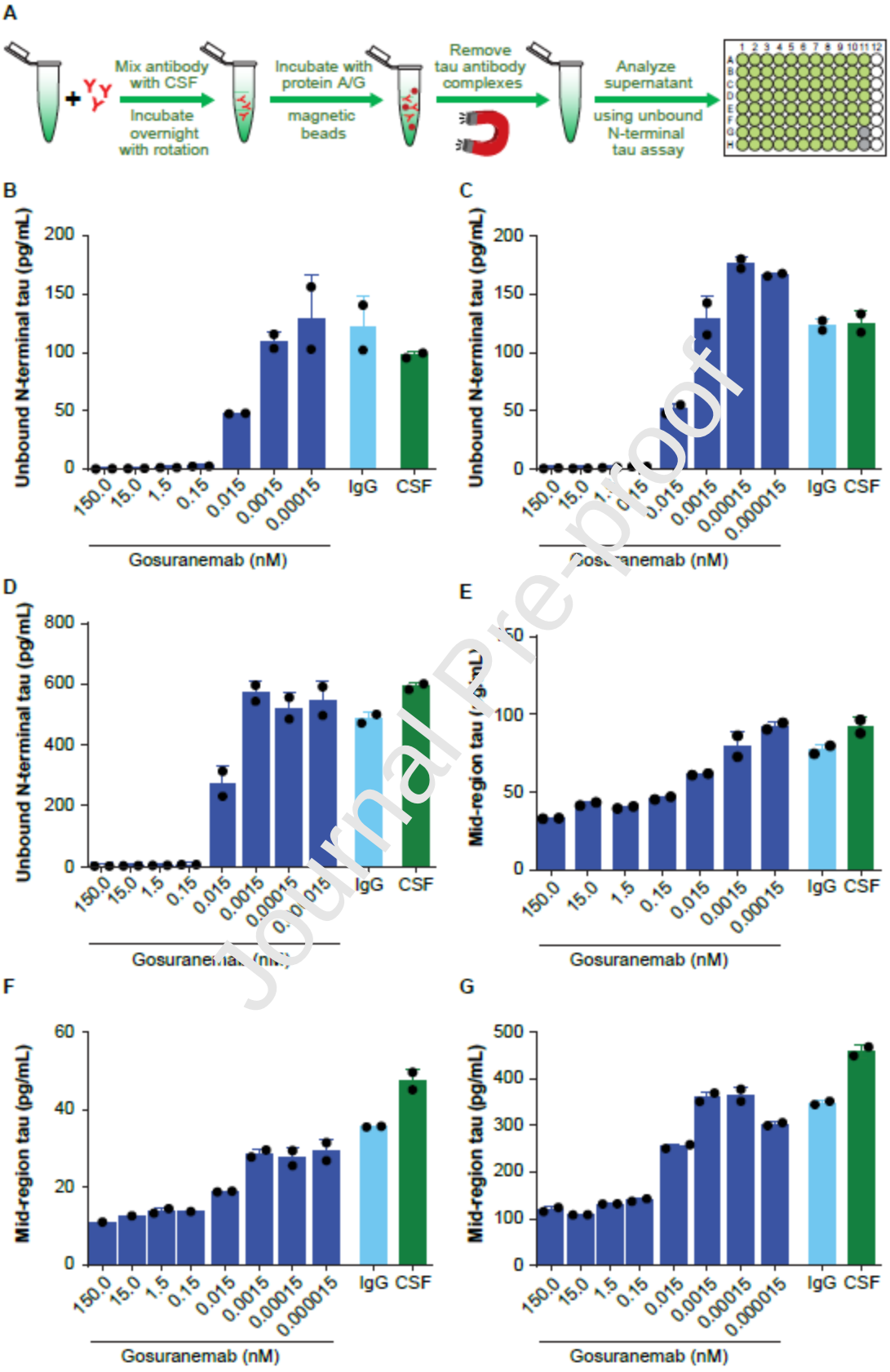

Fig. 8. Gosuranemab binds to extracellular tau in AD, PSP, and HV CSF. (A) Assay schematic. CSF was incubated with the antibody, immune complexes were removed using protein A/G magnetic beads, and supernatants were measured for unbound N-terminal tau (B-D) and mid-region tau (E-G) levels. (B–D) Levels of unbound N-terminal tau measured in CSF immunodepleted with 10-fold serial dilutions of gosuranemab starting at 150 nM: PSP CSF (B); HV CSF (C); AD CSF (D). (E–G) Levels of mid-region tau measured in CSF immunodepleted with 10-fold serial dilutions of gosuranemab starting at 150 nM: PSP CSF (B); HV CSF (C); AD CSF (D). Isotype control antibody (IgG) was added at 150 nM only. Data points indicate technical replicates. Averages, SD and % CV of the technical replicates can be found in Supplementary Table 6. AD, Alzheimer's disease; CSF, cerebrospinal fluid; CV, coefficient of variation; HV, healthy volunteer; PSP, progressive supranuclear palsy.

4. Discussion

On the basis of the hypothesis that a seed-competent, extracellular tau species can transit from cell to cell and propagate tau pathology throughout the brain, multiple passive immunotherapies are being developed with the intent of intervening in tau spread (Jadhav et al., 2019). Gosuranemab has been shown to be well tolerated, exhibit a long half-life, and efficiently engage its intended target, achieving up to 97% reduction in CSF unbound N-terminal tau in some clinical trial dosing cohorts (Boxer et al., 2019; Qureshi et al., 2018). Here we describe a detailed investigation into the structural and functional properties of gosuranemab. Our observations have contributed to a better understanding of the antibody, which will help inform future trials.

We have established that the humanized IPN002 antibody retains high affinity for tau; the monovalent binding affinity of gosuranemab for recombinant tau was determined to be approximately 0.3 nM. Gosuranemab binds both tau monomer and fibril with subnanomolar affinities. In the absence of a clear understanding of the identity and biophysical and biochemical properties of extracellular seed-competent tau, high affinity of gosuranemab for multiple tau forms is advantageous, as it suggests that interaction with extracellular soluble tau and aggregated tau species is possible. While at this point in time, the exact nature of seed-competent tau is unknown, it is clear from the literature that assembly into aggregates requires sequence in the tau MTBR (residues 243-368). Based on multiple reports, very little tau is present in human CSF beyond residue 224 and full-length tau has only been detected at low levels, approximately 1pM (Chen et al., 2019; Guix et al., 2018). While high affinity is undoubtedly important for engaging tau, in particular in the extracellular space where levels of tau seeds are so low, specificity for tau seed may prove critical for efficacious tau immunotherapies in humans. Treatment of preclinical models with various antibodies have hinted that specificity, or epitope, could be key for

reducing tau pathology (Albert et al., 2019; d'Abramo et al., 2013), with the caveat that these studies relied on human tau transgene expression driven by heterologous promoters resulting in tau production at non-physiological levels throughout different brain regions. We examined two of these humanized antibodies (i.e. zagotenemab and UCB0107), alongside two other anti-tau antibodies currently being tested in clinical trials. We show that the gosuranemab variable domain has a higher intrinsic affinity for monomeric tau than tilavonemab, zagotenemab, semorinemab, or UCB0107. In some cases, these lower affinities correlated with reduced binding to insoluble tau (CBD or PSP) relative to gosuranemab. The pattern of aggregated tau can vary between diseases, with variations observed in tau isoform patterns, phosphorylation, and conformation (Arendt et al., 2016). Cryo-electron microscopy has revealed distinctive folds adopted by tau from patients with Pick's disease and CBD, neurodegenerative disorders characterized by 3R tau and 4R tau, respectively (Falcon et al., 2018; Zhang et al., 2020), and AD tau which is comprised of both 3R and 4R tau (Fitzpatrick et al., 2017). This suggests that an additional tau fold might also exist for the 4R tauopathy like PSP. This could translate to inaccessible epitopes for specific antibodies and explain the differences we observed in their binding to disease tau.

The high affinity of gosuranemab for tau from different tauopathies (AD, CBD, and PSP), and its ability to inhibit tau seeding activity of AD and PSP brain homogenates, suggests that the gosuranemab epitope (mapped to residues 15–22 in this study) is present in seed-competent tau species from these tauopathies. Structural models of tau fibrils constructed from cryo-electron microscopy and solid-state nuclear magnetic resonance generally do not show residues 15–22 that are considered dynamic and solvent accessible (Bibow et al., 2011; Daebel et al., 2012; Dregni et al., 2019; Falcon et al., 2018; Fitzpatrick et al., 2017; Lippens and Gigant, 2019; Schwalbe et al., 2014). The binding profile of gosuranemab indicates that it may be able to recognize a variety of different tau conformations found in pathological tau aggregates.

The crystal structure and epitope mapping studies provided detailed insights into the binding properties of gosuranemab. First, we refined the epitope of gosuranemab from that previously reported (Bright et al., 2015) to residues 15–22 of tau. This region of tau is fully conserved between human and cynomolgus monkey, but differs significantly from mouse, rat, dog, or guinea pig. Second, the extensive buried surface area comprising the tau–gosuranemab interface in the crystal structure is consistent with the high affinity of gosuranemab for tau, deduced from binding studies. Third, the crystal structure revealed that tau residues T17 and Y18 are packed tightly at the gosuranemab V*H*/V*L* interface and suggested that this pocket would be unable to accommodate post-translational modifications. pY18 tau

has been detected in the intracellular neurofibrillary tangles of brains of individuals with AD (Lee et al., 2004), and elevated pY18 levels correlate with an increase in phosphorylation at the AT8 epitope, an established marker of tau pathology (Bhaskar et al., 2010; Neddens et al., 2018). Tau Y18 is phosphorylated by Src family kinases Fyn and Lck, which have been implicated in neurodegenerative diseases (Bhaskar et al., 2005; Lee et al., 2004; Scales et al., 2011; Usardi et al., 2011). Tau Y18 is also susceptible to nitration (nY18) and serves as a pathological hallmark for several tauopathies (Reyes et al., 2012; Reyes et al., 2008); however, the significance of nY18 is unknown. For these reasons we chose to investigate gosuranemab binding to modified tau peptides by solution-base binding techniques, i.e. MST. Our crystal structure indicated that gosuranemab-bound $tau_{15–22}$ adopts a beta-turn conformation. Structural studies of full-length tau with NMR and cryoEM (Fitzpatrick et al., 2017; Mukrasch et al., 2009) indicate that the region immediately upstream of the gosuranemab epitope is involved in long-range contacts which potentially stabilize the beta-turn. These long-range contacts and putative stabilizing effects are missing from peptides we used for MST, which could account for the micromolar affinities we measured, rather than nanomolar affinities we observed with SPR and ELISA. Affinities measured with MST have been reported to deviate from those measured using other experimental formats like SPR (Miles et al., 2013). Nevertheless, MST revealed that when tau T17 and Y18 residues were phosphorylated, or Y18 was nitrated, the binding of gosuranemab was dramatically reduced. Although Y18 has been validated as a tau phosphorylation site in human brain tissue using immunocytochemistry, the spatial distribution and function of pY18 tau is primarily intracellular (Kanaan et al., 2012; Lee et al., 2004). Phosphorylated Y18 or nY18 forms of tau in CSF have not been reported, and phosphorylation of extracellular tau from induced pluripotent stem cells-derived cortical neurons was rarely detected at Y18 and only observed at residues T181, S202, and T231 (Bright et al., 2015). The lack of reported T17 and Y18 modifications on extracellular tau suggests that gosuranemab should bind to the majority of extracellular N-terminal tau forms that contain residues 15–22 and should impede tau spreading. Indeed, the seeding activity of AD brain homogenate is completely removed by gosuranemab, indicating that pathological tau seeds are not modified at T17 or Y18.

As shown by us and others, tissue homogenate derived from brains of individuals with AD or PSP can readily induce tau aggregation in cells (Courade et al., 2018; Mirbaha et al., 2015; Sanders et al., 2014; Woerman et al., 2015). We have demonstrated with experiments using biosensor cells that gosuranemab can bind forms of tau thatt seed intracellular tau aggregation, at relevant therapeutic concentrations. Empirical data from clinical trial NCT02460094 showed that serum C_{max} at day 57 for a

2100 mg cohort was 913 µg/mL (Boxer et al., 2019). The gosuranemab CSF:serum ratio was reported to be approximately 0.4% across all doses tested and generally similar between days 29 and 85. Therefore, we expect ~30 nM gosuranemab in CSF. Of note, the same gosuranemab dose (2100 mg) has been used in our phase 2 study of gosuranemab in participants with AD (TANGO, NCT03352557). We derived an IC_{50} range of 25–60 pM and 17–40 pM for gosuranemab in the cellular tau aggregation assays using individual AD and PSP donor brain homogenate, respectively. These concentrations represent approximately 0.1% of the circulating concentration of gosuranemab in NCT02460094 clinical trial CSF. Tilavonemab and UCB0107 performed similarly to gosuranemab in our functional assays using AD brain homogenate, consistent with results from AD brain homogenate binding experiments derived by ELISA. The majority of tau seeds contained in the brain preparations used for our assays, however, are presumably of intracellular origin. Here we have shown for the first time that ISF derived from rTg4510 mice contains seed-competent tau [previously demonstrated for transgenic CSF (Takeda et al., 2016)] and that gosuranemab can completely thwart cellular tau aggregation induced by ISF. Tau (N-terminal and mid-region fragments, and full-length) levels in human CSF are estimated to be approximately 30 pM (Chen et al., 2019; Guix et al., 2018). The molar ratios of gosuranemab:tau used in our biosensor experiments are therapeutically relevant (approximately 100:1 and 200:1 for brain homogenate and transgenic ISF, respectively), less than the predicted molar ratio of gosuranemab:tau in human CSF derived from gosuranemab concentrations measured for a 2100 mg cohort in clinical trial NCT02460094 (1000:1). While these data point at the potential of gosuranemab to impede tau seeding activity, these observations were made using an engineered cell line expressing non-physiological levels of an aggregation-prone mutant tau. Further, our biosensor cell experiments involved immune-complex removal and transfection into cells, when *in vivo* gosuranemab would persist in circulation at levels influenced by pharmacokinetics and depend on physiological mechanisms to potentially be taken up by cells. While we never observed "spontaneous" aggregation in our biosensor cell model, implying a strict criterion for tau seed presence (Supplementary Fig. 5A), the aggregates formed may not reflect the type of aggregate that is present in the brains of patients. These studies may not have generated the aggregate that most closely resembles native aggregation, however they have demonstrated the impact of gosuranemab treatment on seeding related to the specific material used (brain homogenate and ISF).

The ability of gosuranemab to prevent the induction of tau aggregation is not unique to the biosensor cell system because gosuranemab was also able to impede the aggregation of endogenous tau in wildtype mouse primary cortical neurons. We estimate the IC_{50} for gosuranemab to be ~2 µg/mL (14

nM) in this assay, which is approximately half the maximal concentration of gosuranemab in CSF from the NCT02460094 clinical trial 2100 mg cohort. Notably, in this assay the inhibitory effect of gosuranemab treatment appears to reach a maximum of 50%, a similar extent of inhibition as that resulting from treatment with the mid-region recognizing anti-tau Tau5 antibody. We speculate that this plateau of inhibition may result from dissociation of the tau-antibody complex, degradation, or sequestration of the antibody spatially into cellular compartments where it is unable to bind tau. Importantly, the ability of AD-tau to seed tau aggregation in mouse neuronal cells was reduced in the presence of tau–gosuranemab complexes, suggesting that the effect of gosuranemab does not rely on the removal of the immune complex. While the mouse neuron experiments hint at the prospect of gosuranemab as a means with which to impede or slow tau seeding activity, these *in vitro* observations, like those made with the biosensor cell experiments, utilized a simple system devoid of multiple cell types and lacking the complexity of organ tissue. Dosing rTg4510 mice with gosuranemab revealed that virtually all extracellular N-terminal tau is bound to gosuranemab, as evidenced by an inability to detect gosuranemab-unbound tau in both antemortem ISF and CSF. This indicates that gosuranemab can access the brain parenchyma and ISF and that tau binding in ISF correlates with tau binding in CSF. Taken together, along with our biosensor and mouse neuron experiments, our data show that gosuranemab can efficiently bind extracellular tau seeds and potentially block tau spreading. However, as communicated above, cautious interpretation is warranted given that transgenic models are not an accurate reflection of human disease because of the unnatural regulation of the human tau transgene. The experiments described here are unlikely to be completely predictive of *in vivo* efficacy and the treatment benefits of gosuranemab ultimately rely on clinical trial readouts.

Using an ultrasensitive immunoassay to measure mid-region tau, we observed a reduction of approximately 50% in mid-region tau in human CSF after immunodepletion with gosuranemab, irrespective of disease classification, suggesting that half of fragments in CSF have an intact N-terminus. However, using the same platform to measure tau in transgenic mouse ISF and CSF after 8 weekly doses of 60 mg/kg gosuramemab, we found that while nearly all extracellular tau with an intact N-terminal epitope was bound by gosuranemab, the concentration of mid-region tau in transgenic mouse ISF and CSF was not significantly lowered. This is consistent with CSF measurements taken from healthy participants and individuals diagnosed with PSP who were dosed with gosuranemab (Boxer et al., 2019; Qureshi et al., 2018). While our *ex vivo* experiments indicate that likely half of all mid-region tau fragments have an intact N-terminus, the nature of the assay measuring mid-region tau from ISF and

CSF does not distinguish between gosuranemab-bound and gosuranemab-unbound mid-region populations. We demonstrate that gosuranemab can bind full-length tau, conceivably the most likely extracellular culprit accountable for seeding, with subnanomolar affinity, and we expect circulating gosuranemab will engage all full-length tau in CSF with the administered AD phase 2 clinical trial dose (2100 mg).

It is notable that although the preclinical data support gosuranemab as a potential treatment both for primary tauopathies (e.g. PSP) and for secondary tauopathies (e.g. AD), gosuranemab failed to demonstrate a clinical benefit for patients with PSP in the recently completed PASSPORT trial (NCT03068468). On the basis of our characterization of tau binding, the affinity of gosuranemab is unlikely to explain the failure of the PASSPORT trial to reach its primary endpoint, which was a significant change in PSP Rating Scale score from baseline. Gosuranemab is still under investigation for AD (TANGO, NCT03352557), a tauopathy that is pathologically and clinically distinct from PSP. Gosuranemab is thought to target tau pathogenesis that occurs via a spreading mechanism. This mechanism may pertain more to AD, where the pattern of pathologic tau distribution correlates well with age and disease severity, in line with the Braak staging scheme (Arendt et al., 2016; Cope et al., 2018; Nelson et al., 2012). In PSP, pathologic tau deposits are most prominent in the midbrain and deep-brain nuclei early in the course of Richardson's syndrome, the most common clinical variant of PSP (Cope et al., 2018), with spread to cortical regions observed mostly in the advanced stages of the disease (Boxer et al., 2017). In AD, there is a clear correlation of tau burden with clinical symptoms (Nelson et al., 2012), but no such correlation is observed in PSP. Tau pathology in AD is exclusively neuronal, consistent with transneuronal spread (Arendt et al., 2016; Cope et al., 2018). In PSP, on the other hand, pathologic tau species have also been observed in non-neuronal cell types (i.e. astrocytes and oligodendrocytes) (Arendt et al., 2016), suggesting a mechanism beyond neuronal spread. Further, elevation of CSF tau levels in AD, but not PSP, suggests different mechanisms for the diseases (Boxer et al., 2017; Lashley et al., 2018; Shi et al., 2016). Thus, a failure to demonstrate efficacy in the PSP trial cannot be viewed as predictive for the potential outcome of clinical studies in AD.

In conclusion, we have shown that the anti-tau monoclonal antibody, gosuranemab, exhibits high affinity for its intended target, N-terminal tau, and can bind extracellular tau species. The ability of gosuranemab to impede extracellular tau seeds and prevent intracellular tau aggregation, and the tolerability and safety of the antibody observed in clinical trials, provide continued optimism for ongoing trials of gosuranemab and other tau-targeted immunotherapies in AD.

Acknowledgments

Use of the Advanced Photon Source was supported by the U.S. Department of Energy, Office of Science, Office of Basic Energy Sciences, under contract no. DE-AC02-06CH11357. Use of the LRL Collaborative Access Team (LRL-CAT) beam line facilities at Sector 31 of the Advanced Photon Source was provided by Eli Lilly & Company, which operates the facility. Isin Dalkilic-Liddle provided the HEK293T biosensor cell line.

Biogen provided funding for medical writing support in the development of this paper; Ira Probodh from Excel Medical Affairs provided writing support, and Adrienne Trout from Excel Medical Affairs copyedited and styled the manuscript per journal requirements. Biogen reviewed and provided feedback on the paper to the authors. The authors had full editorial control of the paper, and provided their final approval of all content.

Funding

This study was funded by Biogen (Cambridge, MA, USA). The sponsor was involved in the study design; in the collection, analysis, and interpretation of data; in the writing of the report; and in the decision to submit the article for publication.

Declaration of competing interests and financial disclosures

Richelle Sopko, Olga Golonzhka, Joseph Arndt, Chao Quan, Julie Czerkowicz, Benjamin Smith, Yogapriya Murugesan, Paul H. Weinreb, Danielle L. Graham, and Heike Hering are employees of and stockholders in Biogen. Andrew Cameron was an employee of and stockholder in Biogen at the time of this study, and is currently an employee of Voyager Therapeutics, Inc. Garrett Gibbons and Soo-Jung Kim have no conflicts of interest to declare. John Q. Trojanowski, Virginia M.Y. Lee, and Kurt R. Brunden have received research funding from Biogen.

Author contributions

Richelle Sopko: Conceptualization, Methodology, Investigation, Resources, Writing - Review & Editing.
Olga Golonzhka: Conceptualization, Methodology, Investigation, Writing - Review & Editing.
Joseph Arndt: Conceptualization, Methodology, Investigation, Writing - Review & Editing.
Chao Quan: Methodology, Investigation, Writing - Review & Editing.
Julie Czerkowicz: Methodology, Investigation, Writing - Review & Editing.

Andrew Cameron: Methodology, Investigation, Writing - Review & Editing.

Benjamin Smith: Methodology, Investigation, Writing - Review & Editing.

Yogapriya Murugesan: Methodology, Investigation, Writing - Review & Editing.

Garrett Gibbons: Methodology, Investigation, Writing - Review & Editing.

Soo-Jung Kim: Methodology, Investigation, Writing - Review & Editing.

John Q. Trojanowski: Methodology, Supervision, Writing-Review & Editing

Virginia M.Y. Lee: Methodology, Supervision, Writing-Review & Editing

Kurt R. Brunden: Conceptualization, Writing - Review & Editing, Supervision, Project administration, Funding acquisition.

Paul H. Weinreb: Conceptualization, Supervision, Writing - Review & Editing.

Danielle L. Graham: Conceptualization, Supervision, Writing - Review & Editing.

Heike Hering: Conceptualization, Supervision, Writing - Review & Editing.

References

Adams, P.D., Afonine, P.V., Bunkóczi, G., Chen, V.B., Davis, I.W., Echols, N., Headd, J.J., Hung, L.W., Kapral, G.J., Grosse-Kunstleve, R.W., McCoy, A.J., Moriarty, N.W., Oeffner, R., Read, R.J., Richardson, D.C., Richardson, J.S., Terwilliger, T.C., Zwart, P.H., 2010. PHENIX: a comprehensive Python-based system for macromolecular structure solution. Acta Crystallogr. D. Biol. Crystallogr. 66 (Pt 2), 213–221. doi:10.1107/S0907444909052925.

Adolfsson, O., Wildsmith, K., Van der Brug, M., Muhs, A., 2018. Anti-tau antibodies and methods of use. World Intellectual Property Organization, International Publication Number: WO 2018/106776 A2.

Albert, M., Mairet-Coello, G., Danis, C., Lieger, S., Caillierez, R., Carrier, S., Skrobala, E., Landrieu, I., Michel, A., Schmitt, M., Citron, M., Downey, P., Courade, J.P., Buée, L., Colin, M., 2019. Prevention of tau seeding and propagation by immunotherapy with a central tau epitope antibody. Brain. 142, 1736-1750. doi:10.1093/brain/awz100.

Arendt, T., Stieler, J.T., Holzer, M., 2016. Tau and tauopathies. Brain Res. Bull. 126 (Pt 3), 238–292. doi:10.1016/j.brainresbull.2016.08.018.

Barthélemy, N.R., Gabelle, A., Hirtz, C., Fenaille, F., Sergeant, N., Schraen-Maschke, S., Vialaret, J., Buée, L., Junot, C., Becher, F., Lehmann, S., 2016. Differential mass spectrometry profiles of tau protein in the cerebrospinal fluid of patients with Alzheimer's disease, progressive supranuclear palsy, and dementia with lewy bodies. J. Alzheimers Dis. 51, 1033–1043. doi:10.3233/JAD-150962.

Bhaskar, K., Hobbs, G.A., Yen, S.H., Lee, G., 2010. Tyrosine phosphorylation of tau accompanies disease progression in transgenic mouse models of tauopathy. Neuropathol. Appl. Neurobiol. 36, 462–477. doi:10.1111/j.1365-2990.2010.01103.x.

Bhaskar, K., Yen, S.H., Lee, G., 2005. Disease-related modifications in tau affect the interaction between fyn and tau. J. Biol. Chem. 280, 35119–35125. doi:10.1074/jbc.M505895200.

Bibow, S., Mukrasch, M.D., Chinnathambi, S., Biernat, J., Griesinger, C., Mandelkow, E., Zweckstetter, M., 2011. The dynamic structure of filamentous tau. Angew. Chem. Int. Ed. Engl. 50, 11520–11524. doi:10.1002/anie.201105493.

Boxer, A.L., Qureshi, I., Ahlijanian, M., Grundman, M., Golbe, L.I., Litvan, I., Honig, L.S., Tuite, P., McFarland, N.R., O'Suilleabhain, P., Xie, T., Tirucherai, G.S., Bechtold, C., Bordelon, Y., Geldmacher, D.S., Grossman, M., Isaacson, S., Zesiewicz, T., Olsson, T., Muralidharan, K.K., Graham, D.L., O'Gorman, J., Haeberlein, S.B., Dam, T., 2019. Safety of the tau-directed monoclonal antibody BIIB092 in progressive supranuclear palsy: a randomised, placebo-controlled, multiple ascending

dose phase 1b trial. Lancet Neurol. 18, 549–558. doi:10.1016/S1474-4422(19)30139-5.

Boxer, A.L., Yu, J.T., Golbe, L.I., Litvan, I., Lang, A.E., Höglinger, G.U., 2017. Advances in progressive supranuclear palsy: new diagnostic criteria, biomarkers, and therapeutic approaches. Lancet Neurol. 16, 552–563. doi:10.1016/S1474-4422(17)30157-6.

Bright, J., Hussain, S., Dang, V., Wright, S., Cooper, B., Byun, T., Ramos, C., Singh, A., Parry, G., Stagliano, N., Griswold-Prenner, I., 2015. Human secreted tau increases amyloid-beta production. Neurobiol. Aging. 36, 693–709. doi:10.1016/j.neurobiolaging.2014.09.007.

Chen, Z., Mengel, D., Keshavan, A., Rissman, R.A., Billinton, A., Perkinton, M., Percival-Alwyn, J., Schultz, A., Properzi, M., Johnson, K., Selkoe, D.J., Sperling, R.A., Patel, P., Zetterberg, H., Galasko, D., Schott, J.M., Walsh, D.M., 2019. Learnings about the complexity of extracellular tau aid development of a blood-based screen for Alzheimer's disease. Alzheimers Dement. 15, 487–496. doi:10.1016/j.jalz.2018.09.010.

Cicognola, C., Brinkmalm, G., Wahlgren, J., Portelius, E., Gobom, J., Cullen, N.C., Hansson, O., Parnetti, L., Constantinescu, R., Wildsmith, K., Chen, H.H., Beach, T.G., Lashley, T., Zetterberg, H., Blennow, K., Hoglund, K., 2019. Novel tau fragments in cerebrospinal fluid: relation to tangle pathology and cognitive decline in Alzheimer's disease. Acta Neuropathol. 137, 279-296. doi:10.1007/s00401-018-1948-2.

Colin, M., Dujardin, S., Schraen-Maschke, S., Meno-Tetang, G., Duyckaerts, C., Courade, J.P., Buée, L., 2020. From the prion-like propagation hypothesis to therapeutic strategies of anti-tau immunotherapy. Acta Neuropathol. 139, 3–25. doi:10.1007/s00401-019-02087-9.

Cope, T.E., Rittman, T., Borchert, R.J., Jones, P.S., Vatansever, D., Allinson, K., Passamonti, L., Vazquez Rodriguez, P., Bevan-Jones, W.R., O'Brien, J.T., Rowe, J.B., 2018. Tau burden and the functional connectome in Alzheimer's disease and progressive supranuclear palsy. Brain. 141, 550–567. doi:10.1093/brain/awx347.

Courade, J.P., Angers, R., Mairet-Coello, G., Pacico, N., Tyson, K., Lightwood, D., Munro, R., McMillan, D., Griffin, R., Baker, T., Starkie, D., Nan, R., Westwood, M., Mushikiwabo, M.L., Jung, S., Odede, G., Sweeney, B., Popplewell, A., Burgess, G., Downey, P., Citron, M., 2018. Epitope determines efficacy of therapeutic anti-tau antibodies in a functional assay with human Alzheimer tau. Acta Neuropathol. 136, 729–745. doi:10.1007/s00401-018-1911-2.

Crotti, A., Sait, H.R., McAvoy, K.M., Estrada, K., Ergun, A., Szak, S., Marsh, G., Jandreski, L., Peterson, M., Reynolds, T.L., Dalkilic-Liddle, I., Cameron, A., Cahir-McFarland, E., Ransohoff, R.M., 2019. BIN1

favors the spreading of tau via extracellular vesicles. Sci. Rep. 9, 9477. doi:10.1038/s41598-019-45676-0.

Crowe, A., Henderson, M.J., Anderson, J., Titus, S.A., Zakharov, A., Simeonov, A., Buist, A., Delay, C., Moechars, D., Trojanowski, J.Q., Lee, V.M., Brunden, K.R., 2020. Compound screening in cell-based models of tau inclusion formation: Comparison of primary neuron and HEK293 cell assays. J Biol Chem. 295, 4001-4013. doi:10.1074/jbc.RA119.010532.

d'Abramo, C., Acker, C.M., Jimenez, H.T., Davies, P., 2013. Tau passive immunotherapy in mutant P301L mice: antibody affinity versus specificity. PLoS One. 8, e62402. doi:10.1371/journal.pone.0062402.

Daebel, V., Chinnathambi, S., Biernat, J., Schwalbe, M., Habenstein, B., Loquet, A., Akoury, E., Tepper, K., Müller, H., Baldus, M., Griesinger, C., Zweckstetter, M., Mandelkow, E., Vijayan, V., Lange, A., 2012. β-Sheet core of tau paired helical filaments revealed by solid-state NMR. J. Am. Chem. Soc. 134, 13982–13989. doi:10.1021/ja305470p.

Dregni, A.J., Mandala, V.S., Wu, H., Elkins, M.R., Wang, H.K., Hung, I., DeGrado, W.F., Hong, M., 2019. In vitro 0N4R tau fibrils contain a monomorphic β-sheet core enclosed by dynamically heterogeneous fuzzy coat segments. Proc. Natl. Acad. Sci. U S A. 116, 16357–16366. doi:10.1073/pnas.1906839116.

Eftekharzadeh, B., Daigle, J.G., Kapinos, L.E., Coyne, A., Schiantarelli, J., Carlomagno, Y., Cook, C., Miller, S.J., Dujardin, S., Amaral, A.S., Grima, J.C., Bennett, R.E., Tepper, K., DeTure, M., Vanderburg, C.R., Corjuc, B.T., DeVos, S.L., Gonzalez, J.A., Chew, J., Vidensky, S., Gage, F.H., Mertens, J., Troncoso, J., Mandelkow, E., Salvatella, X., Lim, R.Y.H., Petrucelli, L., Wegmann, S., Rothstein, J.D., Hyman, B.T., 2018. Tau protein disrupts nucleocytoplasmic transport in Alzheimer's disease. Neuron. 99, 925–940.e7. doi:10.1016/j.neuron.2018.07.039.

Emsley, P., Lohkamp, B., Scott, W.G., Cowtan, K., 2010. Features and development of Coot. Acta Crystallogr. D. Biol. Crystallogr. 66 (Pt 4), 486–501. doi:10.1107/S0907444910007493.

Fá, M., Puzzo, D., Piacentini, R., Staniszewski, A., Zhang, H., Baltrons, M.A., Li Puma, D.D., Chatterjee, I., Li, J., Saeed, F., Berman, H.L., Ripoli, C., Gulisano, W., Gonzalez, J., Tian, H., Costa, J.A., Lopez, P., Davidowitz, E., Yu, W.H., Haroutunian, V., Brown, L.M., Palmeri, A., Sigurdsson, E.M., Duff, K.E., Teich, A.F., Honig, L.S., Sierks, M., Moe, J.G., D'Adamio, L., Grassi, C., Kanaan, N.M., Fraser, P.E., Arancio, O., 2016. Extracellular tau oligomers produce an immediate impairment of LTP and memory. Sci. Rep. 6, 19393. doi:10.1038/srep19393.

Falcon, B., Zhang, W., Murzin, A.G., Murshudov, G., Garringer, H.J., Vidal, R., Crowther, R.A., Ghetti, B., Scheres, S.H.W., Goedert, M., 2018. Structures of filaments from Pick's disease reveal a novel tau

protein fold. Nature. 561, 137–140. doi:10.1038/s41586-018-0454-y.

Fitzpatrick, A.W.P., Falcon, B., He, S., Murzin, A.G., Murshudov, G., Garringer, H.J., Crowther, R.A., Ghetti, B., Goedert, M., Scheres, S.H.W., 2017. Cryo-EM structures of tau filaments from Alzheimer's disease. Nature. 547, 185-190. doi:10.1038/nature23002.

Fuster-Matanzo, A., Hernández, F., Ávila, J., 2018. Tau spreading mechanisms; implications for dysfunctional tauopathies. Int. J. Mol. Sci. 19, pii: E645. doi:10.3390/ijms19030645.

Gamache, J., Benzow, K., Forster, C., Kemper, L., Hlynialuk, C., Furrow, E., Ashe, K.H., Koob, M.D., 2019. Factors other than htau overexpression that contribute to tauopathy-like phenotype in rTg4510 mice. Nat. Commun. 10, 2479. doi:10.1038/s41467-019-10428-1.

Gibbons, G.S., Banks, R.A., Kim, B., Changolkar, L., Riddle, D.M., Leight, S.N., Irwin, D.J., Trojanowski, J.Q., Lee, V.M.Y., 2018. Detection of Alzheimer disease (AD)-specific tau pathology in AD and nonAD tauopathies by immunohistochemistry with novel conformation-selective tau antibodies. J. Neuropathol. Exp. Neurol. 77, 216–228. doi:10.1093/jnen/nly010.

Gibbons, G.S., Lee, V.M.Y., Trojanowski, J.Q., 2019. Mechanisms of cell-to-cell transmission of pathological tau: a review. JAMA Neurol. 76, 101–108. doi:10.1001/jamaneurol.2018.2505.

Gómez-Ramos, A., Díaz-Hernández, M., Cuadros, R., Hernández, F., Avila, J., 2006. Extracellular tau is toxic to neuronal cells. FEBS Lett. 580, 4842–4850. doi:10.1016/j.febslet.2006.07.078.

Gómez-Ramos, A., Díaz-Hernández, M., Rubio, A., Miras-Portugal, M.T., Avila, J., 2008. Extracellular tau promotes intracellular calcium increase through M1 and M3 muscarinic receptors in neuronal cells. Mol. Cell. Neurosci. 37, 673–681. doi:10.1016/j.mcn.2007.12.010.

Guix, F.X., Corbett, G.T., Cha, D.J., Mustapic, M., Liu, W., Mengel, D., Chen, Z., Aikawa, E., Young-Pearse, T., Kapogiannis, D., Selkoe, D.J., Walsh, D.M., 2018. Detection of Aggregation-Competent Tau in Neuron-Derived Extracellular Vesicles. Int J Mol Sci. 19. doi:10.3390/ijms19030663.

Guo, J.L., Narasimhan, S., Changolkar, L., He, Z., Stieber, A., Zhang, B., Gathagan, R.J., Iba, M., McBride, J.D., Trojanowski, J.Q., Lee, V.M., 2016. Unique pathological tau conformers from Alzheimer's brains transmit tau pathology in nontransgenic mice. J. Exp. Med. 213, 2635–2654. doi:10.1084/jem.20160833.

Guo, T., Noble, W., Hanger, D.P., 2017. Roles of tau protein in health and disease. Acta Neuropathol. 133, 665–704. doi:10.1007/s00401-017-1707-9.

Hill, E., Karikari, T.K., Moffat, K.G., Richardson, M.J.E., Wall, M.J., 2019. Introduction of tau oligomers into cortical neurons alters action potential dynamics and disrupts synaptic transmission and

plasticity. eNeuro. 6, pii: ENEURO.0166-19.2019. doi:10.1523/ENEURO.0166-19.2019.

Holmes, B.B., Furman, J.L., Mahan, T.E., Yamasaki, T.R., Mirbaha, H., Eades, W.C., Belaygorod, L., Cairns, N.J., Holtzman, D.M., Diamond, M.I., 2014. Proteopathic tau seeding predicts tauopathy in vivo. Proc. Natl. Acad. Sci. U S A. 111, E4376–E4385. doi:10.1073/pnas.1411649111.

Jadhav, S., Avila, J., Schöll, M., Kovacs, G.G., Kövari, E., Skrabana, R., Evans, L.D., Kontsekova, E., Malawska, B., de Silva, R., Buee, L., Zilka, N., 2019. A walk through tau therapeutic strategies. Acta Neuropathol. Commun. 7, 22. doi:10.1186/s40478-019-0664-z.

Jicha, G.A., Bowser, R., Kazam, I.G., Davies, P., 1997. Alz-50 and MC-1, a new monoclonal antibody raised to paired helical filaments, recognize conformational epitopes on recombinant tau. J. Neurosci. Res. 48, 128–132.

Kabsch, W., 2010. XDS. Acta Crystallogr. D. Biol. Crystallogr. 66, 125–132. doi:10.1107/S0907444909047337.

Kanaan, N.M., Morfini, G., Pigino, G., LaPointe, N.E., Andreadis, A., Song, Y., Leitman, E., Binder, L.I., Brady, S.T., 2012. Phosphorylation in the amino terminus of tau prevents inhibition of anterograde axonal transport. Neurobiol. Aging. 33, 826.e15–30. doi:10.1016/j.neurobiolaging.2011.06.006.

Karch, C.M., Jeng, A.T., Goate, A.M., 2012. Extracellular tau levels are influenced by variability in tau that is associated with tauopathies. J. Biol. Chem. 287, 42751–42762. doi:10.1074/jbc.M112.380642.

Krissinel, E., Henrick, K., 2007. Inference of macromolecular assemblies from crystalline state. J. Mol. Biol. 372, 774–797. doi:10.1016/j.jmb.2007.05.022.

Kuroda, D., Gray, J.J., 2016. Shape complementarity and hydrogen bond preferences in protein-protein interfaces: implications for antibody modeling and protein-protein docking. Bioinformatics. 32, 2451–2456. doi:10.1093/bioinformatics/btw197.

Lasagna-Reeves, C.A., Castillo-Carranza, D.L., Sengupta, U., Guerrero-Munoz, M.J., Kiritoshi, T., Neugebauer, V., Jackson, G.R., Kayed, R., 2012. Alzheimer brain-derived tau oligomers propagate pathology from endogenous tau. Sci Rep. 2, 700. doi:10.1038/srep00700.

Lashley, T., Schott, J.M., Weston, P., Murray, C.E., Wellington, H., Keshavan, A., Foti, S.C., Foiani, M., Toombs, J., Rohrer, J.D., Heslegrave, A., Zetterberg, H., 2018. Molecular biomarkers of Alzheimer's disease: progress and prospects. Dis. Model. Mech. 11, pii: dmm031781. doi:10.1242/dmm.031781.

Lawrence, M.C., Colman, P.M., 1993. Shape complementarity at protein/protein interfaces. J. Mol. Biol. 234, 946–950. doi:10.1006/jmbi.1993.1648.

Lee, B., Richards, F.M., 1971. The interpretation of protein structures: estimation of static accessibility. J.

Mol. Biol. 55, 379–400. doi:10.1016/0022-2836(71)90324-x.

Lee, G., Thangavel, R., Sharma, V.M., Litersky, J.M., Bhaskar, K., Fang, S.M., Do, L.H., Andreadis, A., Van Hoesen, G., Ksiezak-Reding, H., 2004. Phosphorylation of tau by fyn: implications for Alzheimer's disease. J. Neurosci. 24, 2304–2312. doi:10.1523/JNEUROSCI.4162-03.2004.

Li, W., Lee, V.M., 2006. Characterization of two VQIXXK motifs for tau fibrillization in vitro. Biochemistry. 45, 15692–15701. doi:10.1021/bi061422+.

Lippens, G., Gigant, B., 2019. Elucidating tau function and dysfunction in the era of cryo-EM. J. Biol. Chem. 294, 9316–9325. doi:10.1074/jbc.REV119.008031.

Magnoni, S., Esparza, T.J., Conte, V., Carbonara, M., Carrabba, G., Holtzman, D.M., Zipfel, G.J., Stocchetti, N., Brody, D.L., 2012. Tau elevations in the brain extracellular space correlate with reduced amyloid-β levels and predict adverse clinical outcomes after severe traumatic brain injury. Brain. 135 (Pt 4), 1268–1280. doi:10.1093/brain/awr286.

Mansuroglu, Z., Benhelli-Mokrani, H., Marcato, V., Sultan, A., Violet, M., Chauderlier, A., Delattre, L., Loyens, A., Talahari, S., Bégard, S., Nesslany, F., Colin, M., Souès, S., Lefebvre, B., Buée, L., Galas, M.C., Bonnefoy, E., 2016. Loss of tau protein affects the structure, transcription and repair of neuronal pericentromeric heterochromatin. Sci. Rep. 6, 33047. doi:10.1038/srep33047.

McCoy, A.J., Grosse-Kunstleve, R.W., Adams, P.D., Winn, M.D., Storoni, L.C., Read, R.J., 2007. Phaser crystallographic software. J. Appl. Crystallogr. 40 (Pt 4), 658–674. doi:10.1107/S0021889807021206.

Meredith, J.E., Jr., Sankaranarayanan, S., Guss, V., Lanzetti, A.J., Berisha, F., Neely, R.J., Slemmon, J.R., Portelius, E., Zetterberg, H., Blennow, K., Soares, H., Ahlijanian, M., Albright, C.F., 2013. Characterization of novel CSF tau and ptau biomarkers for Alzheimer's disease. PLoS One. 8, e76523. doi:10.1371/journal.pone.0076523.

Miles, L.A., Crespi, G.A., Doughty, L., Parker, M.W., 2013. Bapineuzumab captures the N-terminus of the Alzheimer's disease amyloid-beta peptide in a helical conformation. Sci Rep. 3, 1302. doi:10.1038/srep01302.

Mirbaha, H., Holmes, B.B., Sanders, D.W., Bieschke, J., Diamond, M.I., 2015. Tau trimers are the minimal propagation unit spontaneously internalized to seed intracellular aggregation. J. Biol. Chem. 290, 14893–14903. doi:10.1074/jbc.M115.652693.

Miyamoto, T., Stein, L., Thomas, R., Djukic, B., Taneja, P., Knox, J., Vossel, K., Mucke, L., 2017. Phosphorylation of tau at Y18, but not tau-fyn binding, is required for tau to modulate NMDA

receptor-dependent excitotoxicity in primary neuronal culture. Mol. Neurodegener. 12, 41. doi:10.1186/s13024-017-0176-x.

Mukrasch, M.D., Bibow, S., Korukottu, J., Jeganathan, S., Biernat, J., Griesinger, C., Mandelkow, E., Zweckstetter, M., 2009. Structural polymorphism of 441-residue tau at single residue resolution. PLoS Biol. 7, e34. doi:10.1371/journal.pbio.1000034.

Narasimhan, S., Guo, J.L., Changolkar, L., Stieber, A., McBride, J.D., Silva, L.V., He, Z., Zhang, B., Gathagan, R.J., Trojanowski, J.Q., Lee, V.M.Y., 2017. Pathological tau strains from human brains recapitulate the diversity of tauopathies in nontransgenic mouse brain. J. Neurosci. 37, 11406–11423. doi:10.1523/JNEUROSCI.1230-17.2017.

Neddens, J., Temmel, M., Flunkert, S., Kerschbaumer, B., Hoeller, C., Loeffler, T., Niederkofler, V., Daum, G., Attems, J., Hutter-Paier, B., 2018. Phosphorylation of different tau sites during progression of Alzheimer's disease. Acta Neuropathol. Commun. 6, 52. doi:10.1186/s40478-018-0557-6.

Nelson, P.T., Alafuzoff, I., Bigio, E.H., Bouras, C., Braak, H., Cairns, N.J., Castellani, R.J., Crain, B.J., Davies, P., Del Tredici, K., Duyckaerts, C., Frosch, M.P., Haroutunian, V., Hof, P.R., Hulette, C.M., Hyman, B.T., Iwatsubo, T., Jellinger, K.A., Jicha, G.A., Kövari, E., Kukull, W.A., Leverenz, J.B., Love, S., Mackenzie, I.R., Mann, D.M., Masliah, E., McKee, A.C., Montine, T.J., Morris, J.C., Schneider, J.A., Sonnen, J.A., Thal, D.R., Trojanowski, J.Q., Troncoso, J.C., Wisniewski, T., Woltjer, R.L., Beach, T.G., 2012. Correlation of Alzheimer disease neuropathologic changes with cognitive status: a review of the literature. J. Neuropathol. Exp. Neurol. 71, 362–381. doi:10.1097/NEN.0b013e31825018f7.

Nobuhara, C.K., DeVos, S.L., Commins, C., Wegmann, S., Moore, B.D., Roe, A.D., Costantino, I., Frosch, M.P., Pitstick, R., Carlson, G.A., Hock, C., Nitsch, R.M., Montrasio, F., Grimm, J., Cheung, A.E., Dunah, A.W., Wittmann, M., Bussiere, T., Weinreb, P.H., Hyman, B.T., Takeda, S., 2017. Tau antibody targeting pathological species blocks neuronal uptake and interneuron propagation of tau in vitro. Am. J. Pathol. 187, 1399–1412. doi:10.1016/j.ajpath.2017.01.022.

Novak, P., Kontsekova, E., Zilka, N., Novak, M., 2018. Ten years of tau-targeted immunotherapy: The path walked and the roads ahead. Front. Neurosci. 12, 798. doi:10.3389/fnins.2018.00798.

Pooler, A.M., Phillips, E.C., Lau, D.H., Noble, W., Hanger, D.P., 2013. Physiological release of endogenous tau is stimulated by neuronal activity. EMBO Rep. 14, 389–394. doi:10.1038/embor.2013.15.

Qureshi, I.A., Tirucherai, G., Ahlijanian, M.K., Kolaitis, G., Bechtold, C., Grundman, M., 2018. A randomized, single ascending dose study of intravenous BIIB092 in healthy participants. Alzheimers Dement. (N Y). 4, 746–755. doi:10.1016/j.trci.2018.10.007.

Ramsden, M., Kotilinek, L., Forster, C., Paulson, J., McGowan, E., SantaCruz, K., Guimaraes, A., Yue, M., Lewis, J., Carlson, G., Hutton, M., Ashe, K.H., 2005. Age-dependent neurofibrillary tangle formation, neuron loss, and memory impairment in a mouse model of human tauopathy (P301L). J Neurosci. 25, 10637–10647. doi:10.1523/JNEUROSCI.3279-05.2005.

Reyes, J.F., Geula, C., Vana, L., Binder, L.I., 2012. Selective tau tyrosine nitration in non-AD tauopathies. Acta Neuropathol. 123, 119–132. doi:10.1007/s00401-011-0898-8.

Reyes, J.F., Reynolds, M.R., Horowitz, P.M., Fu, Y., Guillozet-Bongaarts, A.L., Berry, R., Binder, L.I., 2008. A possible link between astrocyte activation and tau nitration in Alzheimer's disease. Neurobiol. Dis. 31, 198–208. doi:10.1016/j.nbd.2008.04.005.

Sanders, D.W., Kaufman, S.K., DeVos, S.L., Sharma, A.M., Mirbaha, H., Li, A., Barker, S.J., Foley, A.C., Thorpe, J.R., Serpell, L.C., Miller, T.M., Grinberg, L.T., Seeley, W.W., Diamond, M.I., 2014. Distinct tau prion strains propagate in cells and mice and define different tauopathies. Neuron. 82, 1271–1288. doi:10.1016/j.neuron.2014.04.047.

Sankaranarayanan, S., Barten, D.M., Vana, L., Devidze, N., Yang, L., Cadelina, G., Hoque, N., DeCarr, L., Keenan, S., Lin, A., Cao, Y., Snyder, B., Zhang, B., Nitla, M., Hirschfeld, G., Barrezueta, N., Polson, C., Wes, P., Rangan, V.S., Cacace, A., Albright, C.F., Meredith, J., Jr., Trojanowski, J.Q., Lee, V.M., Brunden, K.R., Ahlijanian, M., 2015. Passive immunization with phospho-tau antibodies reduces tau pathology and functional deficits in two distinct mouse tauopathy models. PLoS One. 10, e0125614. doi:10.1371/journal.pone.0125614.

Santacruz, K., Lewis, J., Spires, T., Paulson, J., Kotilinek, L., Ingelsson, M., Guimaraes, A., DeTure, M., Ramsden, M., McGowan, E., Forster, C., Yue, M., Orne, J., Janus, C., Mariash, A., Kuskowski, M., Hyman, B., Hutton, M., Ashe, K.H., 2005. Tau suppression in a neurodegenerative mouse model improves memory function. Science. 309, 476–481. doi:10.1126/science.1113694.

Sato, C., Barthélemy, N.R., Mawuenyega, K.G., Patterson, B.W., Gordon, B.A., Jockel-Balsarotti, J., Sullivan, M., Crisp, M.J., Kasten, T., Kirmess, K.M., Kanaan, N.M., Yarasheski, K.E., Baker-Nigh, A., Benzinger, T.L.S., Miller, T.M., Karch, C.M., Bateman, R.J., 2018. Tau kinetics in neurons and the human central nervous system. Neuron. 97, 1284–1298.e7. doi:10.1016/j.neuron.2018.02.015.

Scales, T.M., Derkinderen, P., Leung, K.Y., Byers, H.L., Ward, M.A., Price, C., Bird, I.N., Perera, T., Kellie, S., Williamson, R., Anderton, B.H., Reynolds, C.H., 2011. Tyrosine phosphorylation of tau by the SRC family kinases lck and fyn. Mol. Neurodegener. 6, 12. doi:10.1186/1750-1326-6-12.

Schwalbe, M., Ozenne, V., Bibow, S., Jaremko, M., Jaremko, L., Gajda, M., Jensen, M.R., Biernat, J.,

Becker, S., Mandelkow, E., Zweckstetter, M., Blackledge, M., 2014. Predictive atomic resolution descriptions of intrinsically disordered htau40 and α-synuclein in solution from NMR and small angle scattering. Structure. 22, 238–249. doi:10.1016/j.str.2013.10.020.

Shi, M., Kovac, A., Korff, A., Cook, T.J., Ginghina, C., Bullock, K.M., Yang, L., Stewart, T., Zheng, D., Aro, P., Atik, A., Kerr, K.F., Zabetian, C.P., Peskind, E.R., Hu, S.C., Quinn, J.F., Galasko, D.R., Montine, T.J., Banks, W.A., Zhang, J., 2016. CNS tau efflux via exosomes is likely increased in Parkinson's disease but not in Alzheimer's disease. Alzheimers Dement. 12, 1125–1131. doi:10.1016/j.jalz.2016.04.003.

Sigurdsson, E.M., 2018. Tau immunotherapies for Alzheimer's disease and related tauopathies: progress and potential pitfalls. J. Alzheimers Dis. 64 (Suppl 1), S555–S565. doi:10.3233/JAD-179937.

Skachokova, Z., Martinisi, A., Flach, M., Sprenger, F., Naegelin, Y., Steiner-Monard, V., Sollberger, M., Monsch, A.U., Goedert, M., Tolnay, M., Winkler, D.T., 2019. Cerebrospinal fluid from Alzheimer's disease patients promotes tau aggregation in transgenic mice. Acta Neuropathol Commun. 7, 72. doi:10.1186/s40478-019-0725-3.

Sugahara, M., Kunishima, N., 2006. Novel versatile cryoprotectants for heavy-atom derivatization of protein crystals. Acta Crystallogr. D. Biol. Crystallogr. 62 (Pt 5), 520–526. doi:10.1107/S0907444906009012.

Takeda, S., Commins, C., DeVos, S.L., Nobuhara, C.K., Wegmann, S., Roe, A.D., Costantino, I., Fan, Z., Nicholls, S.B., Sherman, A.E., Trisini Lipsanopoulos, A.T., Scherzer, C.R., Carlson, G.A., Pitstick, R., Peskind, E.R., Raskind, M.A., Li, G., Montine, T.J., Frosch, M.P., Hyman, B.T., 2016. Seed-competent high-molecular-weight tau species accumulates in the cerebrospinal fluid of Alzheimer's disease mouse model and human patients. Ann Neurol. 80, 355-67. doi:10.1002/ana.24716.

Usardi, A., Pooler, A.M., Seereeram, A., Reynolds, C.H., Derkinderen, P., Anderton, B., Hanger, D.P., Noble, W., Williamson, R., 2011. Tyrosine phosphorylation of tau regulates its interactions with fyn SH2 domains, but not SH3 domains, altering the cellular localization of tau. FEBS J. 278, 2927–2937. doi:10.1111/j.1742-4658.2011.08218.x.

Vanderweyde, T., Apicco, D.J., Youmans-Kidder, K., Ash, P.E.A., Cook, C., Lummertz da Rocha, E., Jansen-West, K., Frame, A.A., Citro, A., Leszyk, J.D., Ivanov, P., Abisambra, J.F., Steffen, M., Li, H., Petrucelli, L., Wolozin, B., 2016. Interaction of tau with the RNA-binding protein TIA1 regulates tau pathophysiology and toxicity. Cell Rep. 15, 1455–1466. doi:10.1016/j.celrep.2016.04.045.

Wagshal, D., Sankaranarayanan, S., Guss, V., Hall, T., Berisha, F., Lobach, I., Karydas, A., Voltarelli, L., Scherling, C., Heuer, H., Tartaglia, M.C., Miller, Z., Coppola, G., Ahlijanian, M., Soares, H., Kramer,

J.H., Rabinovici, G.D., Rosen, H.J., Miller, B.L., Meredith, J., Boxer, A.L., 2015. Divergent CSF τ alterations in two common tauopathies: Alzheimer's disease and progressive supranuclear palsy. J. Neurol. Neurosurg. Psychiatry. 86, 244–250. doi:10.1136/jnnp-2014-308004.

Wang, Y., Mandelkow, E., 2016. Tau in physiology and pathology. Nat. Rev. Neurosci. 17, 5–21. doi:10.1038/nrn.2015.1.

Winn, M.D., Ballard, C.C., Cowtan, K.D., Dodson, E.J., Emsley, P., Evans, P.R., Keegan, R.M., Krissinel, E.B., Leslie, A.G., McCoy, A., McNicholas, S.J., Murshudov, G.N., Pannu, N.S., Potterton, E.A., Powell, H.R., Read, R.J., Vagin, A., Wilson, K.S., 2011. Overview of the CCP4 suite and current developments. Acta Crystallogr. D. Biol. Crystallogr. 67 (Pt 4), 235–242. doi:10.1107/S0907444910045749.

Woerman, A.L., Stöhr, J., Aoyagi, A., Rampersaud, R., Krejciova, Z., Watts, J.C., Ohyama, T., Patel, S., Widjaja, K., Oehler, A., Sanders, D.W., Diamond, M.I., Seeley, W.W., Middleton, L.T., Gentleman, S.M., Mordes, D.A., Südhof, T.C., Giles, K., Prusiner, S.B., 2015. Propagation of prions causing synucleinopathies in cultured cells. Proc. Natl. Acad. Sci. U S A. 112, E4949–E4958. doi:10.1073/pnas.1513426112.

World Health Organization, 2018. WHO drug information: Proposed INN: List 120. 32.

Wu, J.W., Hussaini, S.A., Bastille, I.M., Rodriguez, G.A., Mrejeru, A., Rilett, K., Sanders, D.W., Cook, C., Fu, H., Boonen, R.A., Herman, M., Nahmani, E., Emrani, S., Figueroa, Y.H., Diamond, M.I., Clelland, C.L., Wray, S., Duff, K.E., 2016. Neuronal activity enhances tau propagation and tau pathology in vivo. Nat. Neurosci. 19, 1085–1092. doi:10.1038/nn.4328.

Yamada, K., 2017. Extracellular tau and its potential role in the propagation of tau pathology. Front. Neurosci. 11, 667. doi:10.3389/fnins.2017.00667.

Yamada, K., Cirrito, J.R., Stewart, F.R., Jiang, H., Finn, M.B., Holmes, B.B., Binder, L.I., Mandelkow, E.M., Diamond, M.I., Lee, V.M., Holtzman, D.M., 2011. In vivo microdialysis reveals age-dependent decrease of brain interstitial fluid tau levels in P301S human tau transgenic mice. J. Neurosci. 31, 13110–13117. doi:10.1523/JNEUROSCI.2569-11.2011.

Yamada, K., Holth, J.K., Liao, F., Stewart, F.R., Mahan, T.E., Jiang, H., Cirrito, J.R., Patel, T.K., Hochgräfe, K., Mandelkow, E.M., Holtzman, D.M., 2014. Neuronal activity regulates extracellular tau in vivo. J. Exp. Med. 211, 387–393. doi:10.1084/jem.20131685.

Yanamandra, K., Jiang, H., Mahan, T.E., Maloney, S.E., Wozniak, D.F., Diamond, M.I., Holtzman, D.M., 2015. Anti-tau antibody reduces insoluble tau and decreases brain atrophy. Ann. Clin. Transl. Neurol. 2, 278–288. doi:10.1002/acn3.176.

Zabik, N.L., Imhof, M.M., Martic-Milne, S., 2017. Structural evaluations of tau protein conformation: methodologies and approaches. Biochem. Cell. Biol. 95, 338–349. doi:10.1139/bcb-2016-0227.

Zhang, W., Tarutani, A., Newell, K.L., Murzin, A.G., Matsubara, T., Falcon, B., Vidal, R., Garringer, H.J., Shi, Y., Ikeuchi, T., Murayama, S., Ghetti, B., Hasegawa, M., Goedert, M., Scheres, S.H.W., 2020. Novel tau filament fold in corticobasal degeneration. Nature. 580, 283-287. doi:10.1038/s41586-020-2043-0.

Author contributions

Richelle Sopko: Conceptualization, Methodology, Investigation, Resources, Writing - Review & Editing.

Olga Golonzhka: Conceptualization, Methodology, Investigation, Writing - Review & Editing.

Joseph Arndt: Conceptualization, Methodology, Investigation, Writing - Review & Editing.

Chao Quan: Methodology, Investigation, Writing - Review & Editing.

Julie Czerkowicz: Methodology, Investigation, Writing - Review & Editing.

Andrew Cameron: Methodology, Investigation, Writing - Review & Editing.

Benjamin Smith: Methodology, Investigation, Writing - Review & Editing.

Yogapriya Murugesan: Methodology, Investigation, Writing - Review & Editing.

Garrett Gibbons: Methodology, Investigation, Writing - Review & Editing.

Soo-Jung Kim: Methodology, Investigation, Writing - Review & Editing.

John Q. Trojanowski: Methodology, Supervision, Writing-Review & Editing

Virginia M.Y. Lee: Methodology, Supervision, Writing-Review & Editing

Kurt R. Brunden: Conceptualization, Writing - Review & Editing, Supervision, Project administration, Funding acquisition.

Paul H. Weinreb: Conceptualization, Supervision, Writing - Review & Editing.

Danielle L. Graham: Conceptualization, Supervision, Writing - Review & Editing.

Heike Hering: Conceptualization, Supervision, Writing - Review & Editing.

Highlights

- Gosuranemab, an anti-tau antibody, is being studied for Alzheimer's disease.
- Gosuranemab bound to tau with high affinity.
- Gosuranemab inhibited pathologic tau–induced tau aggregation in cells.
- Structure/activity of gosuranemab–tau complex showed that the epitope was $tau_{15–22}$.
- Gosuranemab bound extracellular tau in interstitial and cerebrospinal fluid.